



Common Borders. Common Solutions.

**A Scientific Network
for Earthquake, Landslide & Flood Hazard Prevention**



Current Status Assessment

(Investigation on the potential use of remotely sensed data (satellite images) to gather information related to landslide, seismic and flood hazards)

**Deliverable No.: D.01.02
GA 1. Current Status Assessment, Activity A1.10**

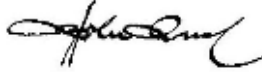
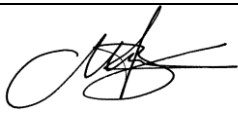
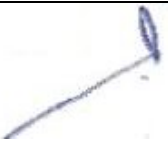
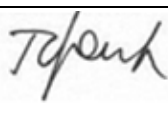
RESPONSIBLE: KOERI (IPA Beneficiary)

INVOLVED PARTNERS: ALL

Project Details

Programme	Black Sea JOP
Priority and Measure	Priority 2 (Sharing resources and competencies for environmental protection and conservation), Measure 2.1. (Strengthening the joint knowledge and information base needed to address common challenges in the environmental protection of river and maritime systems)
Objective	Development of a Scientific Network
Project Title	A Scientific Network for Earthquake, Landslide and Flood Hazard Prevention
Project Acronym	SCInet NatHaz
Contract No	MIS-ETC 2614
Lead Partner	TEI OF KENTRIKI MAKEDONIA, GREECE
Total Budget	700.000,00 Euro (€)
Time Frame	
Start Date - End Date	01/05/2013 - 30/11/2015
Book Captain: Contributing Authors:	K. PAPTAEODOROU (TEI KENTRIKI MAKEDONIA) Konstantinos Papatheodorou, konstantinos Ntours,

Document Release Sheet

Book captain:	A.ANSAL (IPA - BU-KOERI)	 15.11.2015
Approval	K. PAPATHEODOROU (TEI CENTRAL MACEDONIA)	 15.11.2015
Approval	A.ANSAL (IPA - BU-KOERI)	 15.11.2015
Approval	N. KLIMIS (Partner 1 - DUTH)	 15.11.2015
Approval	V. MARGARIS (Partner 2 - EPPO)	 15.11.2015
Approval	V. NENOV (Partner 3 - Burgas Assen Zlatarov University)	 15.11.2015
Approval	L. TOFAN (Partner 4 - Ovidius University of Constanta)	 15.11.2015
Approval	A.SIDORENKO (Partner 5 - IEEN “D.GHITU” Of Academy Of Sciences Of Moldova)	 15.11.2015
Approval	K. STEPANOVA (Partner 6 - Ukranian Environmental Academy Of Sciences, Black Sea Branch)	 15.11.2015
Distribution:	ALL PARTNERS	

RECORD of REVISIONS

Issue/Rev	Date	Page(s)	Description of Change	Release
-	03.11.2013	9	Release of final Template Template prepared by K. NTOUROS	I.01
	01.12.2014	35	Input by Konstantinos Ntouros	I.02
	20.12.2014	55	Input by Konstantinos Papatheorou	I.03
	15.11.2015	55	Review and input by Konstantinos Papatheorou & Konstantinos Ntouros	I.04
	15.11.2015	55	Final Version	I.05

TABLE OF CONTENTS

1	<u>BACKGROUND OF THE DOCUMENT</u>	7
1.1	SUMMARY	7
1.2	SCOPE AND OBJECTIVES	7
2	<u>SATELLITES AND SENSORS</u>	8
3	<u>REMOTE SENSING AND NATURAL HAZARDS</u>	14
3.1	EARTHQUAKES	14
3.2	FLOODS	19
3.3	LANDSLIDES	25
4	<u>REMOTE SENSING IN THE PROJECT’S FRAMEWORK</u>	34
4.1	REMOTE SENSING ANALYSIS TO IMPROVE LANDSLIDE HAZARD ASSESSMENT PERFORMANCE	35
4.1.1	INTRODUCTION – SCOPE	35
4.1.2	MATERIALS AND DATA	37
5	<u>REFERENCES</u>	42
6	<u>ANNEX I – SATELLITE SENSORS</u>	48

LIST OF FIGURES

FIG1. GUI OF USGS EARTH EXPLORER (SEARCH CRITERIA).....	12
FIG2. GUI OF USGS EARTH EXPLORER (DATA SELECTION).....	13
FIG3. GUI OF USGS EARTH EXPLORER (SEARCH RESULTS AND DATA DOWNLOAD).....	14

FIG4. GEOLOGIC MAPS AND TECTONIC REGIME OF SERRES (LEFT) AND NYMFAIA (RIGHT) PILOT IMPLEMENTATION AREAS. FAULT TRACES DIGITIZED FROM GEOLOGIC MAPS PRODUCED BY THE INSTITUTE OF GEOLOGICAL & MINERAL EXPLORATION, GREECE..... 38

FIG. 5 NYMFAIA PILOT IMPLEMENTATION AREA. BAND RATIOS –INVERSED IMAGES (LEFT TO RIGHT): TM4/TM3, TM5/TM3, TM7/TM3, SHOWING LARGE LINEAMENTS (CENTER) WITH WSW-ENE; SW-NE AND NW-SE DIRECTIONS. LANDSAT TM AND ETM+ DATA (NASA) WERE DOWNLOADED FROM [HTTP://GLCF.UMD.EDU/DATA/LANDSAT/](http://GLCF.UMD.EDU/DATA/LANDSAT/) 40

FIG6. FALSE COLOR COMPOSITES (FCC): TM7-TM3-TM1 (LEFT) AND TM4-TM5-TM3 (RIGHT) USED TO TRACE LINEAMENTS AND MAP FRACTURED ZONES IN ROCKS (NYMFAIA PIA). 41

FIG7. TECTONIC REGIME OF SERRES AND NYMFAIA PILOT IMPLEMENTATION AREAS. MAJOR ROAD AXES IN BOTH AREAS SHOWN IN PURPLE. FAULT TRACES DIGITIZED FROM GEOLOGIC MAPS (BLACK LINES) AND FRACTURES MAPPED USING REMOTE SENSING TECHNIQUES (RED LINES). (GEOLOGIC MAPS PRODUCED BY THE INSTITUTE OF GEOLOGICAL & MINERAL EXPLORATION, GREECE). 41

LIST OF TABLES

TABLE 3.3.1 INDICATIVE MINIMUM LANDSLIDES SIZE (M) THAT CAN BE RECOGNIZED UNDER DIFFERENT BACKGROUND CONTRAST AND IMAGE SPATIAL RESOLUTIONS. ALL UNITS ARE IN METERS (M)..... 26

TABLE 3.3.2 MINIMUM AREA SIZE (M²) OF LANDSLIDES NEEDED FOR A LANDSLIDE TO BE IDENTIFIED OR INTERPRETED, DEPENDING ON THE CONDITIONS OF CONTRAST 26

TABLE 3.3.3. AN OVERVIEW OF TECHNIQUES FOR THE COLLECTION OF LANDSLIDE INFORMATION USING REMOTE SENSING DATA 28

TABLE 3.3.4. MAIN SOURCES FOR DIGITAL ELEVATION MODELS 29

TABLE 3.3.5. ENVIRONMENTAL FACTORS AND THEIR RELEVANCE FOR LANDSLIDE SUSCEPTIBILITY AND HAZARD ASSESSMENT 32

TABLE 4.1 OVERVIEW OF EO DATA AVAILABILITY AND THEIR APPLICABILITY..... 34

1 BACKGROUND OF THE DOCUMENT

1.1 SUMMARY

The aim of this chapter was to investigate the potential use of Remote Sensing (RS) in the domain of natural hazards (earthquakes, floods and landslides). According to that, a brief review of the available bibliography was performed in order to identify the advantages and limitations of spaceborne imagery in the field of natural disasters. Moreover, this document contains a list of EO data needs and the valuable information that can be derived from the analysis of satellite imagery based on the selected (different) methodologies for the aforementioned hazards. Remote sensing can play an important role in each of the four phases of the disaster management cycle (mitigation, preparedness, response and recovery). This document focused primarily on the preparedness and mitigation phases

Finally, this chapter acts as an input to the upcoming project's group of activities, namely GA3 “Pilot Implementation in Local and Regional Scales” of the selected methodologies.

1.2 SCOPE AND OBJECTIVES

The spatial nature of the disaster phenomena reveals the importance to the geo-spatial information integration into the decision making process, as regards hazard (earthquakes, floods and landslides) prevention and mitigation actions.

The last fifteen years, remote sensing has increasingly used in the field of natural disasters due to the increasing development of geospatial technologies (EO satellite programs; geospatial data production and analysis techniques) along with World Wide Web expansion, for timely information delivery [1], [2].

In order to assess the use of remote sensing in the field of natural hazards (earthquakes, floods and landslides), a bibliographic overview was performed. In this context, the following sections contain a summary of the characteristics of some sensors used in hazards mapping and monitoring, as well as image processing techniques for the assessment of different types of hazards.

This overview will act as a guide for the implementation of RS techniques in (ELF) hazard assessment within the framework of the project.

The specific objectives of this chapter can be summarized as follows:

- Recording of available satellites and sensors

- Overview of image processing techniques for the assessment of different types of hazards
- Assessment of the suitability and applicability of RS and EO data for the project's scopes.

2 SATELLITES AND SENSORS

Since 2000, a large number of satellite earth observation programs were implemented providing that way valuable information about earth surface changes. For this reason, a short overview of the successfully launched EO missions is presented in this section in order to be identified their capabilities and to be utilized in the domain of natural hazards. In the table (**Table 2.1**) - Annex I, the most commonly used satellite sensors and their characteristics are listed. Moreover, in **Table 2.2** - Annex I, information regarding the satellite sensors used for mapping and monitoring different hazard types are summarized.

An additional importance issue that has to be mentioned is the availability of EO imagery, which can also be used to provide data regarding natural hazard assessment..

According to Evangelidis et.al, 2014 [3], *“in recent years, Earth Observation (EO) data have become available from governmental agencies as a result of the ever increasing technological capabilities of the web. Several web portals that provide options for data search, order and download, are identified, such as:”*

- NASA’s Earth Observing System Data and Information System (EOSDIS) [<https://earthdata.nasa.gov/>] which is the core capability for exploring and managing multi source NASA’s Earth data. In relation to data search and acquisition there are several options to discover the data of interest which are: near real-time data products from the MODIS, OMI, AIRS, and MLS instruments, from the Land Atmosphere Near real-time Capability for EOS (LANCE)[<https://earthdata.nasa.gov/data/near-real-time-data>]; The directory level information from the Global Change Master Directory (GCMD)[<http://gcmd.nasa.gov/index.html>] that provides search capabilities by specific field of interest (e.g. agriculture, atmosphere, etc.); instruments; platforms; providers; projects etc.; Cross-Data Center searches through Reverb (<http://reverb.echo.nasa.gov>), a client web service for search and ordering cross-discipline data from all of EOS Clearing House (ECHO) metadata holdings, which facilitates even those users without EO data knowledge and experience; Custom client software using ECHO metadata repository (<https://earthdata.nasa.gov/echo/>) and NASA’s Data Centers specific search*

*Current Status Assessment - Investigation
on the potential use of remotely sensed data*

- tools and services (<https://earthdata.nasa.gov/data/data-tools>) which have developed in order to provide unique services for users of a particular type of data like USGS Earth Explorer (<http://earthexplorer.usgs.gov/>).
- ii) European’s Space Agency (ESA) Earthnet Online portal (<https://earth.esa.int>) which provide services for search and request of EO data from ESA EO Missions (ERS-1, ERS-2, Envisat, GOCE, SMOS, CryoSat), Third Party Missions (TPMs), ESA Campaigns, the GMES Space Component (GSC), SENTINEL-1 and SENTINEL-2 missions as well as sample and auxiliary data from a number of missions and instruments. The Data browsing can be performed by mission and instrument, or by Earth topic, typology and processing level.
 - iii) Canadian Space Agency provides capabilities of searching and downloading open access data (Canada’s Open Data portal) [<http://data.gc.ca/eng>] which are comprising and EO data over Canada such as Landsat imagery. The data search can be performed through free text form and filters by Organization, Data Type and Subject etc.
 - iv) National Remote Sensing Center (NSRC) of Indian Space Research Organization (ISRO) distributes open EO Data archive of ISRO’s satellite products (Resourcesat-1: Ortho AWiFS and LISS III data; IMS-1: HySI Spectral Binned data) for India via the Bhuvan geoportal (<http://bhuvan.nrsc.gov.in>).
 - v) Argentina’s National Commission on Space Activities (CONAE) provides catalogue imagery data search under different state of access and downloading (<http://www.conae.gov.ar/index.php/es/catalogo-de-imagenes>).
 - vi) Brazilian’s National Institute for Space Research (INPE) has a catalogue search imagery products (CEBERS, Landsat, MODIS TERRA, MODIS AQUA, Resourcesat-1) as well as provides the capability of imagery data acquisition after registration (<http://www.dgi.inpe.br/CDSR/>).

Moreover, several projects/initiatives can be found at literature dealing with EO data access and management through WEB.

- i) The Digital Earth Community project (GENESI –DEC) aims to facilitate the world wide user communities to have access to EO data using a single access point through a simple web portal and web services (<http://www.genesi-dec.eu>).
- ii) The Grid Processing on Demand (G-POD) for Earth Observation Applications initiative provides a grid based platform where the user can search the available data products (ERS-1 and ERS-2 satellites, and the

*Current Status Assessment - Investigation
on the potential use of remotely sensed data*

- Envisat ASAR and MERIS sensors) as well as to exploit the platform's tools and algorithms in order to process the selected data (<http://gpod.eo.esa.int/>).*
- iii) The Global Earth Observation Grid (GEO Grid) [<http://www.geogrid.org>] project provides a platform for worldwide Earth Sciences community including among others a set of services for accessing remote sensing (ASTER; MODIS) and geologic data. Access of data can be performed through a geoportal (<https://eco.geogrid.org/gridsphere/gridsphere>).*
- iv) The Global Earth Observation System of Systems (GEOSS) aims to develop an international infrastructure for EO data access and that way to provide decision support tools to a wide range of users in nine societal benefit areas (disaster management, health, energy, climate, water, weather, ecosystems, agriculture, and biodiversity). The GEOSS Common Infrastructure (GCI) facilitates the end users to access, search and use the data, information, tools and services through a web interface (GEO portal) [<http://www.geoportal.org>].*
- v) EUROGEOSS project is the European contribution to GEOSS and provides an initial operating capability for a European Environment Earth Observation System in the three strategic areas of Drought, Forestry and Biodiversity. The data are available via a single access point, the EuroGEOSS Broker (<http://www.eurogeoss-broker.eu/>)*

As it mentioned earlier, there are quite enough repositories for EO imagery search and download and some of them provide the data free of charge. For example USGS Earth Explorer (<http://earthexplorer.usgs.gov/>) provides an easy way for data search, display and acquisition.

The following paragraph describes in brief the procedural steps that have to be followed in order to perform EO data search and download..

- Procedural steps for EO imagery search and acquisition:
 1. Access the USGS Earth Explorer website, using the following address <http://earthexplorer.usgs.gov/>
 2. Free registration is needed to download data.
 3. After registering, login.
 4. EO Data Search: The GUI for the data search is simple and three (3) main steps have to be followed
 - **Search criteria:** In this tab have to be defined the area of interest in order to narrow the search results of the available data. The area of

*Current Status Assessment - Investigation
on the potential use of remotely sensed data*

interest can be defined by using either a “place name” (e.g. like Google maps search) or using specific coordinates, which is provided with two options. The “map option” (use map) allows to enter the specific coordinates using the right pane of screen in order to draw a point or a polygon (area of interest) otherwise you can enter the coordinates manually using the “add coordinates” option. Also, you can specify the area of interest using spatial vector file (shapefile or KML) after uploading it to the platform. Finally, you can also restrict your search results using a date range.

- **Data sets:** Use this tab in order to specify the EO imagery of your interest from the available data catalogue that provided by the platform repository. The data selection can be performed with a simple click on the checkboxes of the desired datasets. In relation to the available datasets, some of them provided free of charge or some can have use restrictions. Generally, as regards global coverage, DEM’s (SRTM and ASTER); Landsat imagery (TM 4-5, +ETM 7 and OLI/TIRS 8) and EO1 (Hyperion and ALI) are available at no cost.
- **Additional criteria:** This is an optional tab in which you can specify criteria in order to limit the search results such as cloud cover percentage of the scene, the level of image processing (e.g. terrain corrected), day or night condition of the scene and imagery of a specific sensor of the selected satellite.
- **Results:** After the definition of your search criteria, click on the ‘results’ button or the ‘results’ tab in order to start the search procedure. The results of the available data of your choice will be presented in this tab.

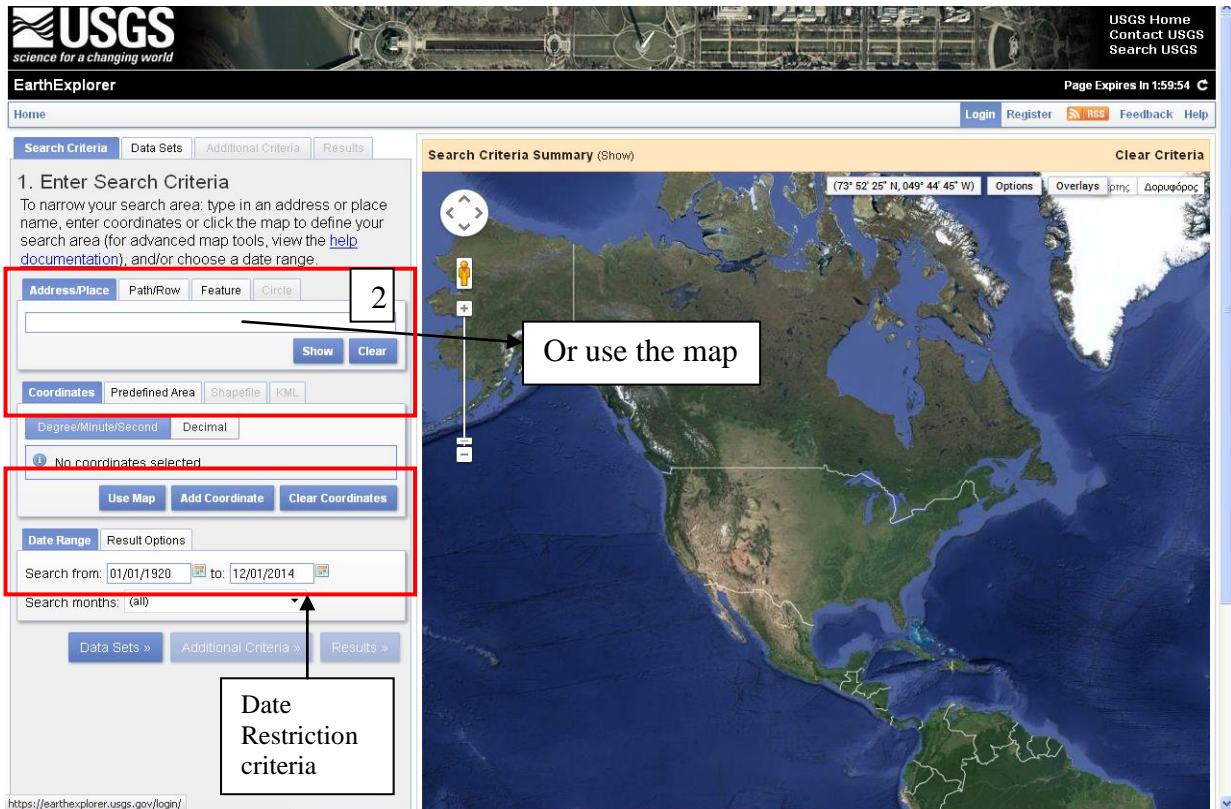


Fig1. GUI of USGS Earth Explorer (search criteria)

5. Search results review and Download: In the results tab there are some options in order to perform data review and finally to download the EO data.
 - Imagery preview: click on the image snapshot in order to preview the image data and the metadata information.
 - Footprint button: provides the area on the map that is covered by the selected scene
 - Image overlay: Overlays the satellite image on the map (right pane of the platform window)
 - Download: Allows to download the selected scene

*Current Status Assessment - Investigation
on the potential use of remotely sensed data*

- Bulk download: provides a mass download procedure by adding the selected images in the “basket”.

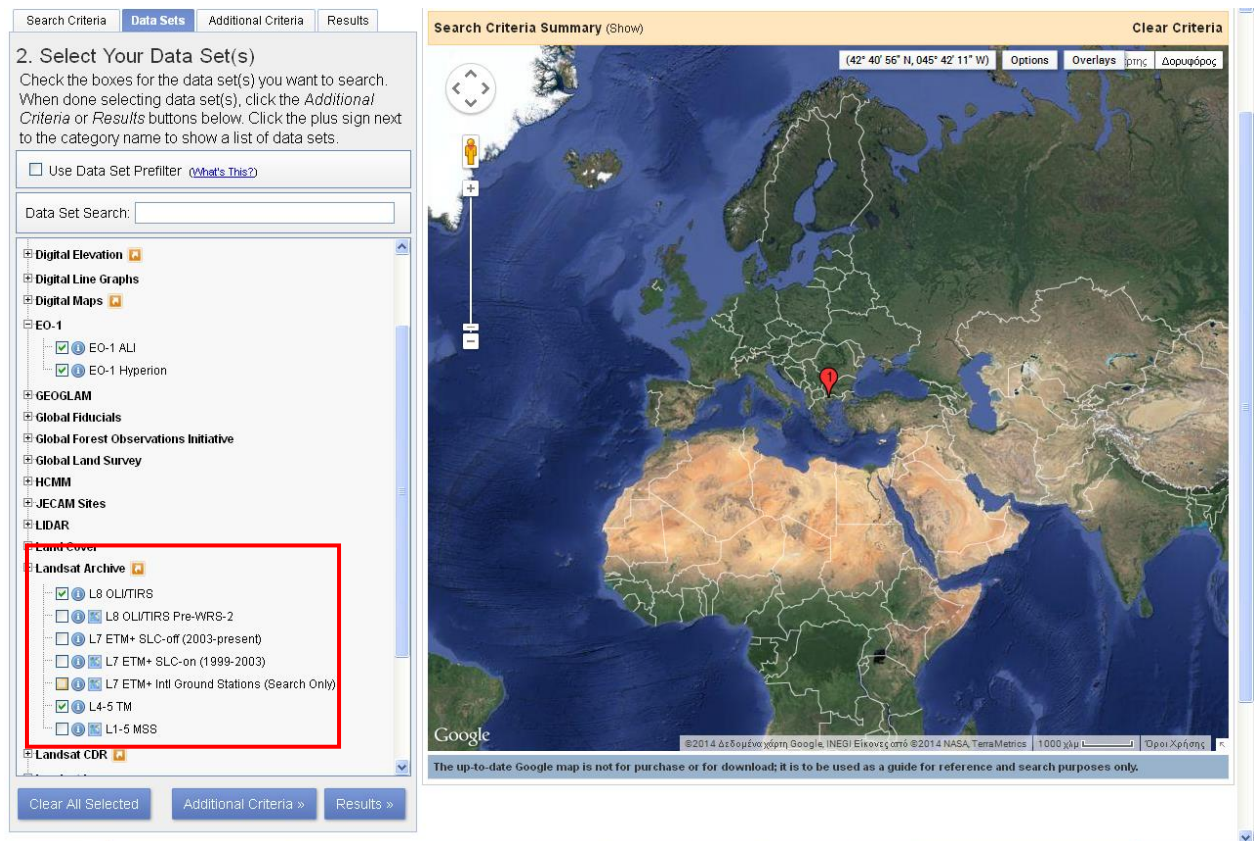


Fig2. GUI of USGS Earth Explorer (data selection)

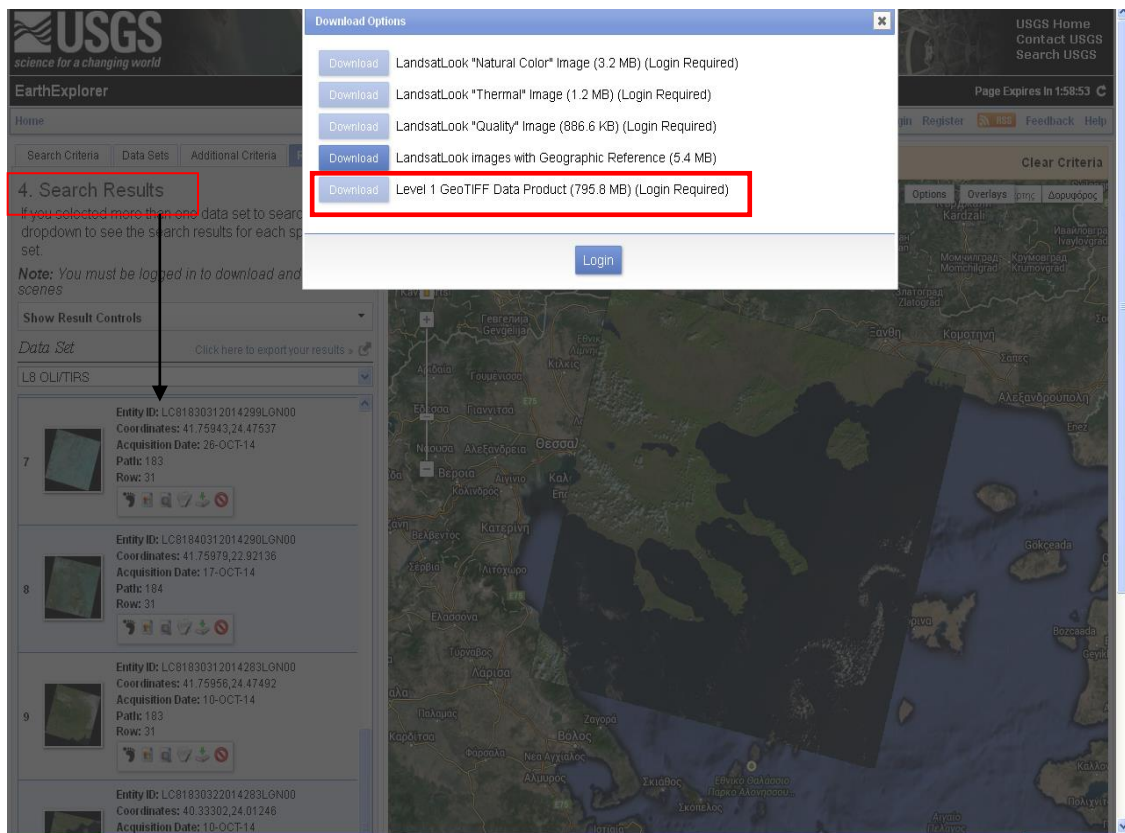


Fig3. GUI of USGS Earth Explorer (search results and data download)

3 REMOTE SENSING AND NATURAL HAZARDS

In this section, an overview of the available bibliography is presented in relation to remote sensing data used as well as image analysis techniques for natural hazards assessment.

3.1 EARTHQUAKES

In the case of earthquakes, the EO (Earth Observation) data use is limited to disaster response and damage assessment phases and at the moment does not provide significant help in the previous mitigation phases (Prevention, Preparedness) despite the fact that effort is being made in research regarding earth crust deformation monitoring.

*Current Status Assessment - Investigation
on the potential use of remotely sensed data*

In the response phase, EO data can be used for damage mapping and consequently to contribute to mobilization of emergency services as well as to better coordination of search and rescue.

Optical remote sensing data (VHR – Very High Resolution) such as IKONOS, Quickbird etc and or with high temporal resolution (e.g. RapidEye), can be used for damage assessment since they provide images with spatial resolution ranging from 0.6 – 1m, but their contribution can be limited due to weather conditions (e.g. cloud coverage).

In practice, a widely used technique for damage mapping in urban environments is the visual interpretation of VHR images [4, 5, 6]. However, manual photo interpretation method has some disadvantages, since it's a time consuming procedure and its results rely heavily on the analyst's experience.

The image visual interpretation can be performed either using pairs of pre – event and post - event imagery or just only the post – event imagery. According to Dong and Shan (2013) [7], different research works can be found in the literature regarding earthquake damage mapping using visual image interpretation; Saito et.al. (2004) [5] used three IKONOS images acquired before and after the Gujarat earthquake (India) and the results were validated using ground survey data; Saito and Spence (2005) [8] used Quickbird images in order to compare the results from only post-event images with those from pre- and post-event images visual interpretation, and concluded that the building damage tended to be underestimated when only post-event images were used; Yamazaki et al. (2005) [9] used Quickbird images and revealed that the pre-event imagery was more helpful in detecting lower building damage grades in comparison when using only post – event images and the detection rate is lower than those of high damage grades.

Except from visual image interpretation, change detection techniques are widely used for earthquake damage assessment. These techniques can be grouped into two categories: i) image enhancement which comprises mathematical operations such as band subtraction and band ratios, principal component analysis and ii) post - classification comparison which allows the identification of changes by comparing two independent image classification results (pre – and post event images) [7].

Change detection techniques can in some cases, not be performed due to presence of shadows, variations in solar illumination and geometric distortions [10]. Yusuf et al. (2001) [11] used Landsat 7 ETM+ panchromatic images before and after the earthquake of Gujarat, India, in order to detect the affected areas by subtracting the reflection intensity (digital number) of the two images.

Zhang et al. (2003) [12] proposed a methodology which is based on image structure features. The damage level was detected by thresholding the differences of the mean

*Current Status Assessment - Investigation
on the potential use of remotely sensed data*

gray scale and the mean variance of the pre- and post-event images. Also, image texture (*texture refers to the spatial variation of image tone as a function of scale*) differences were used for discrimination of damaged and undamaged buildings [7]. Rathje et al. (2005) [13] used co-registered pre- and post-event Quickbird images in order to identify damage patterns in the city of Bam (Iran earthquake) by performing texture change detection algorithm (correlation coefficient). Tomowski et al. (2010) [14] applied four different texture-based change detection approaches (contrast, correlation, energy and Inverse distance moment) to QuickBird images. Through the comparison of the four approaches, the results showed that the best results could be achieved using principal component analysis with the “energy” texture feature.

As regards image classification techniques, object based classification methods are less affected by registration problems in comparison to pixel based (spectral) ones.

The main advantage of classification methods is that the effect of radiometric differences between the multi-temporal data is minimized, but the reliability of the results is based on the accuracy of the initial images classification [7]. Moreover, according to Gillespie et al. (2007) [2], object-oriented classification techniques enhance the quantitative analysis of traditional pixel-based (spectral) methods for change detection in urban environment. Bitelli et al. (2004) [16] performed building damage classification, object-based change detection approach, into different grades using pre- and post-event IRS and QuickBird imagery. Gusella et al. (2005) [17], in order to quantify collapsed buildings, proposed an object-based method, based on the statistical characteristics and an overall accuracy of 70.5% was achieved when performed to pre- and post-earthquake QuickBird images. Li et al. (2009) [18] combined spectral and spatial information for building damage assessment using QuickBird images and the results revealed that the combined information improves significantly the detection rate as compared with the results obtained by using spectral information alone.

Apart from optical imagery, Synthetic Aperture Radar (SAR) images have been used in damage detection caused by earthquakes. Their usage can not be limited due to weather conditions (e.g. cloud coverage) and can be exploited even at building level damage, since the newly developed very high resolution (VHR) radar sensors like TerraSAR-X and COSMO-SkyMed can provide images at a resolution of about 1 m.

According to Dong and Shan (2013) [7], change detection methods in SAR images are based on “amplitude” and “phase” information and generally there are three procedural steps that have to be followed: image despeckling, pixel-by-pixel comparison of two images, and image thresholding.

The “amplitude” information refers to the measure of the strength of the signal, and building damages can be assessed through changes in backscatter coefficient

*Current Status Assessment - Investigation
on the potential use of remotely sensed data*

(backscatter is the portion of the outgoing radar signal that the target redirects directly back towards the radar antenna. It is a measure of the reflective strength of a radar target. The normalised measure of the radar return from a distributed target is called the “backscatter coefficient”, or “sigma nought”, and is defined as per unit area on the ground) and intensity correlation using pre- and post -event SAR images.

The difference of the backscattering coefficient (pre–post event) becomes higher and negative while the correlation coefficient becomes lower in the area showing high damage ratios. On the other hand, in the area with low damage ratios, the difference of the backscattering coefficients becomes lower and the correlation coefficient becomes higher [19]. Matsuoka and Yamazaki (2004) [19], used (before and after event) ERS/SAR images and found that the backscattering coefficients and intensity correlations were notably lower in damaged areas. Also they developed a method for automatic damage detection based on statistical analysis (discriminant analysis). The results were compared with field survey data and showed good agreement.

Chini et al. (2008) [20] in order to detect surface changes that were caused by the 2004 Indonesia earthquake, they used ERS and ENVISAT/ASAR images (before and after the event), took advantage of the backscattering and correlation coefficients and the results agreed with ground-based data. Also, statistical approaches have been used on pre- post event pairs of SAR images [21].

The “phase” information, from multi-temporal SAR images before and after the event, is sensitive to change in building shape due to seismic damage [7]. Coherence imagery (the degree of correlation of the phase information between the two images) was used for damage assessment; damaged areas were identified due to temporal de-correlation that revealed with the use of coherence imagery [22]. Matsuoka and Yamazaki (2000) [23] using pre- and post-event ERS/SAR imagery, found that the degree of coherence (indicates the correlation between two co-registered complex SAR images by calculating the phase of the backscattering echo) can be used for detection of slight to moderate building damages. Hoffmann (2007) [24] revealed that the changes of interferometric coherence derived from pre- and post-event ENVISAT/ ASAR images have closely agreement with independent damage assessments from the IKONOS imagery. Moreover, hybrid methods have been used by combining “amplitude” and “phase” information. Yonezawa et al. (2001) [25] indicated that coherence is of great importance for detection of damaged urban areas by SAR data, especially in the case of damages in which backscattering characteristics do not change.

The direct comparison of optical and SAR data in the domain of damage assessment can not been performed since they have totally different radiometric and physical image formation characteristics. Many researchers have been proposed the use of multi – source (optical, SAR and DEM) remote sensing data for damage building

*Current Status Assessment - Investigation
on the potential use of remotely sensed data*

identification [7]. Stramondo et al. (2006) [10] found better damage classification results that derived from optical images in comparison with SAR in both cases (Izmit, Turkey and Bam, Iran earthquakes), while the combination of optical and SAR imagery (coherence) provided more accurate results compared to SAR or optical data alone. Chini et al. (2009) [26], concluded that the results from the SAR data were improved by using a VHR optical image. Dell'Acqua et al. (2011) [27], used SAR (COSMO/SkyMed) and optical (QuickBird and IKONOS) data and the results shown that optical data were more suitable for indicating damaged and undamaged areas, while SAR image data is more appropriate for distinguishing the extent of the damage at the block scale.

In the preparedness phase, the vulnerability of a landscape to earthquake hazard can be modelled with the combination of different sources of data such as remote sensing imagery (fault mapping; land use/land cover), geologic formations, demographic data, building inventory etc.[2], [15].

As regards fault mapping, optical remote sensing imagery has been extensively used for the detection of tectonic lineaments and the most used technique is the manual image interpretation [1]. Walker (2006) [28] used wide available data, ASTER images and DEM data (SRTM) to mapping the active faults of Kerman province, Iran. Papatheodorou has mapped faults and fractures in rock and verified their presence using ancillary data [66]. Fu et al. (2004) [29] utilized ASTER imagery (before and after the event) in order to identify the fault of Bam earthquake in Iran. The results showed, that the fault extended 65 km through the Bam-Baravat region and potential damage from this earthquake could were been identified in advance.

Image interpretation is heavily based on the analyst experience and is a time consuming process. Except from image interpretation, semi –automated techniques for fault detection can be found in the literature. These methods are based on spatial filtering (edge detection; edge enhancement) [2], [30], [31], [32], but further processing is required such as thresholding.

Moreover, remote sensing imagery and specifically SAR imagery can be utilized for mapping ground deformation caused by earthquakes. According to Joyce et al., (2009) [1] “DInSAR (*Differential Interferometric Synthetic Aperture Radar*) is generally accepted as the best method for earthquake associated deformation mapping”. Also, SAR data can be combined with GPS and seismic data in order provide spatially continuous deformation with sub-centimeter accuracy [15].

3.2 FLOODS

Remote sensing in conjunction with GIS plays an important role in flood modelling, monitoring and management almost from early 90's. According to disaster management cycle, remote sensed data can be used in the “response” phase for inundation area mapping and assessment as well as in the “recovery” phase for integration of remote sensing–derived flood information into models.

Optical remote sensing data have been used for flood mapping. Different techniques are utilized for inundated areas mapping such as image visual interpretation and therefore digitization of water – land boundaries; single band methods; image spectral enhancement (spectral ratios) in order to discriminate water - dry pixels (binary maps); supervised image classification as well as image clustering (unsupervised classification).

Generally, the limitation of the use of optical remote sensing data is due to cloud cover during floods especially in flood cases of small to medium catchments where water often recede prior improvement of the weather conditions; and the fact that flooded areas can not be mapped under the dense vegetation.[33],[1]. Sandholt et al. (2003) [34] used Landsat ETM+ and AVHRR imagery and they concluded that Landsat images can be used for monitoring flooded areas, but the remaining challenge is of obtaining cloud free images.

Although AVHRR imagery has coarse spatial resolution than other commercial imagery, their temporal resolution provides the ability of acquisition cloud free images.

Different image analysis techniques have also been tested; such as supervised classification (Maximum Likelihood) and image clustering (ISODATA) and they showed that no technique is better than the other but each has advantages and limitations depending on the flooding extent, cloud cover and temporal variability.

As regards image enhancement, bands ratios were used for flood mapping – separation wet and dry areas. Wang et al. (2002) [35] showed that the NDVI value for flooded areas remains negative while the value for non-inundated surface is commonly greater than 0. Nevertheless, the use of this threshold is critical since the flooding conditions varies greatly from place to place and the difficulties of selecting the appropriate threshold depends on water surface albedo (increases significantly due to high concentration of sediment in the flooded water) and bare soil decreases considerably due to its high moisture content.

In contrast, other studies showed that the NDVI values of flood areas were significantly positive (Barton et al., 1989) [36] Thus, the use of the “NDVI” approach might not be universally effective in delineating inundated areas [37]. McFeeters

(1996) [38] introduced the Normalized Difference Water Index (NDWI) [Green – NIR/Green +NIR] for the delineation of open water surfaces. This index was developed in order to take advantage of the difference in spectral response of water, vegetation and soil features, namely to maximize water reflectance (Green wavelength); to minimize the low reflectance of water features in the NIR and to exploit of the high reflectance of vegetation and soil features in the NIR. Thus, water features have positive values and consequently are enhanced, while vegetation and soil features have zero or negative values and hence are suppressed [38].

However, NDWI introduces noise in water areas with a built-up background, which means urban features also have positive values in the NDWI image [39]. Xu (2006) [39] modified the NDWI by substituting NIR with MIR and introduced the MNDWI [Green – MIR/Green +MIR] which resulted to noise removal of urban areas. Moreover, other band ratios that were used for delineation of water areas are the ratio band (NIR/MIR) [40] and the ratio bands (Green/ NIR) and (Green/MIR) [41]. Wang et al., (2002) [42] using LANDSAT TM pair images (before and after a flood event) by exploiting the formula (TM7+TM4) for mapping flood extent.

Except for the image enhancement techniques, the single band method can also be used. This method is based on the selection of a single band of a multispectral image to extract water information and then a threshold is determined in order to discriminate water features from land. The limitation of this method is the subjective threshold selection that leads to an over or under estimation of flooded areas and the extracted water information is often affected by shadow noise [39].

Jain et al., (2005) [43] in order to map flooded areas in the Koa catchment India, used IRS LISS III and Landsat TM images and a range of image processing techniques such as density slicing (single band thresholding), Tasseled Cap transformation and Normalized Difference Water Index (NDWI). They concluded that NDWI approach produces best results.

According to Joyce et al., (2009) [1] the use of passive remote sensing sensors data for mapping of flooded areas could be considered ideally, since SAR backscatter signatures between water and vegetation is so distinctive and apart of weather capabilities (cloud penetration), the main advantage is its ability of sharply separation between land and water features. Also SAR backscatter intensity and InSAR coherence can be combined in order to delineate flooding areas. Moreover, InSAR coherence can be used for the estimation of the depth of water in flooded areas as well as the combination of SAR and DEM's.

The most common used technique in active remote sensing as regards delineation of flooded and non flooded areas is radar image thresholding. The thresholds are

*Current Status Assessment - Investigation
on the potential use of remotely sensed data*

identified by a number of processes depending on the study area and overall spectral signature of the imagery.

Change detection techniques have also been used to map flooded areas by using pairs of images (before and after event). Change detection methods in SAR images can be performed on “amplitude” and “phase” information. In the amplitude approach, regions are delineated as flooded where the backscatter, before and after flood event image, is observed to decline significantly.

In coherence approach, the flooded areas identified where the coherence or correlation of radar backscatter (before and after flood event imagery) are very low.

Another technique that can be consider more simple than those mentioned above is the false color composite method using multi – date SAR images. The composite image provides the ability of flood progress monitoring during a specific time period [37].

Another advantage of using SAR images for flood mapping is their ability to detect areas of flooding under vegetation canopy. Flooded areas under vegetation produce enhanced backscatter (bright) in contrast to non flooded areas (under vegetation canopy) due to a double bounce effect. The effect is wavelength - type of vegetation dependent. Additional factors affecting the ability to discriminate flooded areas from the non-flooded ones under a vegetation canopy include the combination of wavelength, incidence angle and polarization.

Finally, the detection of flooded areas under vegetation requires experience on visual interpretation, or the assistance of an image acquired before the flood event for comparison reasons [1], [37]. Nevertheless, some problems can be encountered in relation to the mapping accuracy of flooded areas using SAR images. These problems are related to radar wavelength and to surface roughness or water areas. Under normal conditions, still, calm waters appear in dark tones in SAR images in contrast to rough water surfaces that appear in brighter tones. So, windy conditions over the study area and the associated ripples in the water surface frequently create difficulties to determine the threshold value and thus to delineate the flooded areas.

Another obstacle is the effect of shadows especially in mountainous areas. Yang et al. (1999) [44] overcame this problem by using data fusion of Landsat TM and SAR images. Another way to overcome this problem is by Also, the separation of the flooded and non-flooded in urban environments is also problematic. Generally, the high backscatter of the buildings overlays the backscatter of water within the built-up areas [37].

New technologies and products continuously emerge and provide additional tools for greater efficiency in flood disaster prevention and management actions. Copernicus

*Current Status Assessment - Investigation
on the potential use of remotely sensed data*

system developed by the European Space Agency (ESA), comprising of pairs of satellites called Sentinels provides information regarding land coverage. These Sentinel missions possess arrange of technologies including radar and multispectral imaging for land, ocean and atmospheric monitoring.

There are currently two Sentinel missions launched with a third one about to be launched. Sentinel-1 is a polar orbiting, all-weather, day-and-night radar imaging mission for land and ocean monitoring. Sentinel-2 is a polar orbiting, multispectral, high resolution imaging mission for land monitoring and provides imagery for applications including vegetation mapping, soil and water cover, inland waterways and coastal areas. This kind of data is very useful to map flooded areas and in case of a regular data inflow, to also map flood propagation. Sentinel mission data are available online (<https://sentinel.esa.int/web/sentinel/sentinel-data-access>) and there's even (30.11.2015) a step-by-step guide to use Sentinel data in order to map floods at (<http://www.un-spider.org/advisory-support/recommended-practices/recommended-practice-flood-mapping/step-by-step>).

As regards the “mitigation” phase, mapping of flood hazard and risk is of crucial importance for flood management. According to Sanyal and Lu (2004) [37] flood depth is considered as the most important factor of hazard intensity and is used for the development of flood hazard and risk maps. The estimation of flood depth can be derived from hydrologic data as well as from remotely sensed data and DEM's. High flood depth is associated with high discharge which is a determinant factor of flood severity and consequential damages.

The determination of flood depth using remote sensing data it is not an easy procedure. Islam and Sadu (2001) [45] estimated flood depth using NOAA AVHRR imagery and DEM. They used the tonal difference of the flood water and classified the flooded area into different flood depth zones using supervised classification. This method relies on the analyst experience regarding training areas selection for the classification of different inundation zones and can not be used for local scale mapping due to coarse spatial resolution of imagery.

Another approach of flood depth estimation was proposed by Sanyal and Lu (2005) [46]. They used Landsat ETM+ image acquired during the flood, and performed Principal Component Analysis (PCA) in order to overcome the inter-band correlation since optical bands, except blue band, are very high correlated with the turbidity and sediment concentration of the water. Deeper water has more turbidity than shallower waters because of its high velocity. They found that the best FCC image for flood depth zones delineation was derived by using PC2, PC1 and PC3 bands (RGB).

Moreover, SAR images in conjunction with DEM data can be used for water depth estimation of flood areas. Geudtner et al., (1996) [47] used InSAR coherence

*Current Status Assessment - Investigation
on the potential use of remotely sensed data*

information for estimation of inundation depth. They compared coherence information of a SAR pair images acquired before and during flooding with pair of SAR images that are both acquired before flooding.

A completely different approach for estimation of flood depth was performed by Townsend and Walsh (1998) [48] using the Topographic Wetness Index (TWI) which developed by Beven and Kirkby (1979) [49]. The method is based on terrain morphometric characteristics and the assumption that the water accumulation in a particular point depends upon the area of the upslope region contributing water to that point. The TWI can be produced with the use of hydrologic procedures within a GIS environment by using only as input data DEM's. The limitation of this method is that cannot be performed in flat areas and that it is strongly dependent on the DEM's accuracy.

In the literature there are different works dealing with flood - prone areas mapping using TWI [50], [51]. Other approaches that integrate remote sensing data in order to assist flood hazard and risk assessment can be found in the literature.

Van Der Sande et al. (2003) [52] used VHR imagery (IKONOS-2) in order to produce a detailed land cover map which was used in turn as input data for the flood simulation model to produce a Manning roughness coefficient spatial distribution map of inundated areas. The image was classified with the use of object - based classification method.

Pradhan (2010) [53] produced flood susceptibility maps using geospatial data, ancillary data and remote sensing data (RADARSAT) and performing logistic regression analysis as well as multi-criteria evaluation techniques were used for flood hazard and risk maps production [54]. Finally remote sensing data can be exploited for hydraulic models validation [55], [56].

A “generic” procedure to map flood extent is given at the “KNOWLEDGE PORTAL” of the United Nations Office for Outer Space Affairs UN-SPIDER (<http://www.un-spider.org/advisory-support/recommended-practices/recommended-practice-flood-mapping/in-detail>). The process is based on SAR data which, because as has already been stated, SAR (synthetic aperture radar) measurements from space are independent of daytime and weather conditions and can provide valuable information to monitoring of flood events, due to the fact that smooth water surface provides no returns in the microwave spectrum so it appears black in SAR imagery.

The recommended in the UN “KNOWLEDGE PORTAL” practice, focuses on a simple threshold method for deriving flood extent from SAR imagery.

The basic requirements include:

*Current Status Assessment - Investigation
on the potential use of remotely sensed data*

Data requirements: SAR images (current and possible archived) in Level1, and DEM for ortho-rectification. (a high resolution DEM). Additionally, optical imagery, land cover / land use maps with vector data on infrastructure are beneficial.

For SAR image processing, there's dedicated software (SNAP) freely available from <http://step.esa.int/main/download/> (registration required). For visualization, there's a multitude of available GIS software including Open Source software and Google Earth (<https://www.google.com/earth/explore/products/>).

Skills requirements: basic to intermediate knowledge of image processing; basic knowledge of SAR theory.

Hardware requirements: for processing real SAR images, at least 2 GB of RAM on a fairly modern PC because processing time can be highly reduced since the proposed software SNAP is parallelised.

Potential Applications on flood extend mapping:

- Operational estimation and detection of flooded areas (within 6-12 hours after data acquisition).
- Damage assessment of flooded assets.
- Calibration of hydrometeorological models.
- Detection of water levels using high-resolution DEM.
- Spatial extent: from villages to global scale.
- Can be used for all stages: risk assessment, operational mapping and response, recovery.
- Spatial resolution to mapped areas: Depends on the DEM used and the scale of implementation. Ranges from 1 m to 150 m.

Strengths and Limitations

The use of threshold method for SAR has the following advantages:

- Cloud independent SAR images.
- High revisit time.
- Easy and reliable detection of smooth water.
- Accuracy: up to 95% (depending on the landscape and area).

Limitations:

Deliverable-No. D.01.02 – Activity A.10
Issue: **I.05** Date: 15th November 2015

Final version
Page: **24 of 55**

- Potential false alarm from shadows (variable terrain), smooth objects (like roads) and sand.
- Difficulties in detection floods in urban areas.
- Difficulties in detecting flooded vegetation. (For flooded vegetation detection from SAR data, two multi-temporal images are usually required.)

General description of the workflow:

- (0) SAR image acquisition.
- (1) Calibration in SNAP through Radiometric Correction.
- (2) Speckle filtering in SNAP.
- (3) Binarization in SNAP through Band Math
- (4) Geometric correction in SNAP through Range Doppler Terrain Correction Function.
- (5) Visualization in Google Earth or any GIS software including Open Source.

3.3 LANDSLIDES

Among the main data layers that are required for landslide susceptibility hazard and risk assessment, are landslide inventory data which are considered the most important as it provide insight into the location of landslide phenomena, the types, failure mechanisms, causal factors, frequency of occurrence, volumes and the damage that has been caused. These data can be divided into four main categories including: Landslide inventory data; environmental factors; triggering factors; and elements at risk. Since landslide inventories are either incomplete or completely missing in most countries and high cost in time and money to compile such inventories is extremely restrictive, remote sensing data can be the main source of information for the development of landslide inventories [62].

Both optical and radar imagery can be used for landslide detection and mapping. In the domain of optical remote sensing data (airborne and spaceborne), visual interpretation of single image and stereoscopic images has been extensively used in the past and still is an effective method for landslide detection and mapping [1].

A key issue for landslides detection and mapping using remote sensing data is the data spatial resolution in relation to the size of the features (landslides) as well as the

*Current Status Assessment - Investigation
on the potential use of remotely sensed data*

contrast (the difference in spectral characteristics between the landsides and the surrounding area) [57].

The contrast depends on the period elapsed since the failure because erosion processes and vegetation recovery tend to obscure the "trace" which landslide left on the ground surface; and the severity with which the morphology, drainage and vegetation conditions have been affected by the landslide [58].

Mantovani et al. (1996) [57] have mentioned the minimum sizes of landslide features needed to be recognised for various conditions of contrast background (table 3.3.1). Moreover, Soeters and van Westen (1996) [58] provides the minimum area size of landslides needed for a landslide to be identified or interpreted, depending on the conditions of contrast (table 3.3.2). Nowadays, VHR images from different sensors (World-View, Geo-eye, Pleiades) with spatial resolution from 0.5m to 2m are provided and that way can be used for landslide mapping up to scale of 1: 2000 [59].

Table 3.3.1 Indicative minimum landslides size (m) that can be recognized under different background contrast and image spatial resolutions. All units are in meters (m)

	Landsat MSS	Landsat TM	SPOT multispectral	SPOT Panchromatic	Aerial photos 1:50000	Aerial photos 1:25000	Aerial photos 1:10000
Spatial resolution	80	30	20	10	0.5	0.25	0.1
High contrast	800	300	200	100	5	2.5	1
Low contrast	3200	1200	800	400	20	10	4

(Source: Mantovani, Franco, Robert Soeters, and C. J. Van Westen. "Remote sensing techniques for landslide studies and hazard zonation in Europe." Geomorphology 15.3 (1996): 213-225)

Table 3.3.2 Minimum area size (m²) of landslides needed for a landslide to be identified or interpreted, depending on the conditions of contrast

		Landsat MSS	Landsat TM	SPOT multispectral	SPOT Panchromatic	Aerial photos 1:50000	Aerial photos 1:15000
Spatial resolution (m)		80	30	20	10	1	0,3
High	Identification	160.000	22.500	10.000	2.500	25	6,5

*Current Status Assessment - Investigation
on the potential use of remotely sensed data*

contrast	Interpretation	288.000	40.500	18.000	4.500	45	11,5
Low contrast	Identification	7.040.000	990.000	440.000	110.000	1100	300
	Interpretation	11.520.000	1.620.000	720.000	180.000	1800	450

(Source: Soeters, R., and C. J. van Westen. "Slope Instability Recognition, Analysis and Zonation" in Turner, A.K and Schuster, R.L., (Eds): *Landslides: Investigation and mitigation. Transportation Research Board, Special Report 247. Washington, DC: National Academy Press (1996).*

Nichol and Wong, (2005) [60] used pan-sharpened IKONOS imagery to identify landslides in Hong Kong and they concluded that the image quality of IKONOS image was comparable to that obtained from aerial photos at scale of 1:10.000 providing that way detailed interpretation of landslides. Moreover, Nichol et al. (2006) [61] refers that pan – sharpened IKONOS stereo – imagery can be exploited for interpretation of recent landslides as small as 2–3 m in width.

Nevertheless, manual photo interpretation is a time consuming method and can not be automated. For this reason different approaches can be found in the literature regarding more automated extraction techniques using spaceborne multispectral images.

These methods take advantage of a number of features such as *disrupted or absent vegetation cover (anomalous with the surrounding terrain); slope characteristics; surface characteristics and surface drainage characteristics* [62]. Cheng et al. (2004) [63] used multi-temporal SPOT images and band ratios (NIR/R) in order to locate landslides by land cover change detection.

Moreover, change detection, post classification comparison were performed using multi -temporal SPOT imagery and the results shown almost 70% overall accuracy but detailed boundary delineation of landslides it is not possible due the spatial resolution of used imagery [60].

Other methods, except change detection, have been used such as unsupervised classification and supervised classification and spectral indices thresholding.

Dymond et al. (2006) [64] used SPOT- 5 image data in order to mapping the combined erosion scar and debris of a landslide. The analysis was restricted to slopes greater than 5° in an effort to reduce misclassification of 'bright' pixels (bare land). The analysis showed an accuracy of 80%, but only landslides greater than 10 000 m² were validated.

Joyce et al., (2008) [65] evaluated different semi - automated techniques using SPOT - 5 imagery data. The results revealed that supervised image classification (Spectral

**Current Status Assessment - Investigation
on the potential use of remotely sensed data**

Angle Mapper - SAM) and NDVI thresholding were more accurate techniques (76% accuracy) compared with the results achieved from other used classifiers (parallelepiped, minimum distance to means), principal components, and multi-temporal image differencing (change detection) but visual interpretation of panchromatic SPOT images proved the most accurate technique when compared to field survey (92%).

An overview of techniques for the collection of landslide information using remote sensing data (airborne and spaceborne) is presented in the following table (Table 3.3.3).

Table 3.3.3. An overview of techniques for the collection of landslide information using remote sensing data

Group	Technique	Description	Scale			
			Regional	Medium	Large	detailed
Image interpretation	Stereo aerial photographs	Analog format or digital image interpretation with single or multi-temporal data set	M	H	H	H
	High Resolution satellite images	With monoscopic or stereoscopic images, and single or multi-temporal data set	M	H	H	H
	Radar images	Single data set	L	M	M	M
(Semi) automated classification based on spectral characteristics	Aerial photographs	Image rationing, thresholding	M	H	H	H
	Medium resolution multi-spectral images	Single date images, with pixel based image classification or image segmentation	H	H	H	M
		Multiple date images, with pixel based image classification or image segmentation	H	H	H	M
	Using combinations of	Either use image fusion techniques or	M	M	M	M

**Current Status Assessment - Investigation
on the potential use of remotely sensed data**

	optical and radar data	multi-sensor image classification, either pixel based or object based				
(Semi) automated classification based on altitude characteristics	InSAR	Radar Interferometry for information over larger areas	M	M	M	M
		Permanent scatterers for pointwise displacement data	H	H	H	H
	LiDAR	Overlaying of LiDAR DEMs from different periods	L	L	M	H
	Photogrammetry	Overlaying of DEMs from airphotos or high resolution satellite images for different periods	L	M	H	H
H=highly applicable, M=moderately applicable, and L=Less applicable						

(Source: van Westen, Cees J., Enrique Castellanos, and Sekhar L. Kuriakose. "Spatial data for landslide susceptibility, hazard, and vulnerability assessment: an overview." *Engineering geology* 102.3 (2008): 112-131)

Some other methods for landslide mapping are based on the use of Digital Elevation Models (DEM) of the same area from two different time periods.

Displacements due to landslides can be visualized using DEMs subtraction and displacement volumes can be quantified as well. Accurate Digital Elevation Models (DEM) can be extracted from very high resolution data (VHR) such as Quickbird and IKONOS stereo imagery for detection of large and moderately large landslides [62].

Light Detection and Ranging (LiDAR) data is providing high resolution topographic information (<1m horizontal and few cm vertical accuracy), but is more expensive than the aforementioned spaceborne VHR imagery [1].

In the following table (Table 3.3.4) are presented the main sources for Digital Elevation Models used in landslide hazard and risk assessment studies.

Table 3.3.4. Main sources for Digital Elevation Models

Method	Examples	Scale of analysis			
		Small	Medium	Large	detailed

**Current Status Assessment - Investigation
on the potential use of remotely sensed data**

Contour map derived DEMs	1:100,000 (40 m cont.int)	Hillshading Physiography Internal relief Drainage density	TG	TG	TG
	1:25,000 (10 m cont.int)	Hillshading Physiography Internal relief Drainage density	DEM derivatives: slope steepness, aspect, length, convexity etc.	TG	TG
	1:10,000 (5 m cont.int)	TD	DEM derivatives: slope steepness, aspect, length, convexity etc.	Slope angles, Flow accumulation, Run out modelling	TG
	1:5000 (2 m cont.int)	TD	TD	Slope angles, Flow accumulation, Run out modelling	Slope angles, Flow accumulation, Run out modelling
Medium resolution Satellite derived DEMs	SRTM (30–90 m pixel)	Hillshading Physiography Internal relief Drainage density	TG	TG	TG
	ASTER (15 m pixel)	Hillshading Physiography Internal relief Drainage density	DEM derivatives: slope steepness, aspect, length, convexity etc.	TG	TG
High Resolution	Quickbird, IKONOS (1–4	TD	DEM derivatives:	Slope angles,	Slope angles,

**Current Status Assessment - Investigation
on the potential use of remotely sensed data**

Satellite derived DEMs	m)		slope steepness, aspect, length, convexity etc.	Flow accumulation, Run out modelling, Change detection	Flow accumulation, Run out modelling, Change detection
InSAR	RADARASAT, ENVISAT etc.	TD	Landslide monitoring, Change detection	Landslide monitoring, Change detection	Landslide monitoring, Change detection
LiDAR	ALTM, ALS (1 m DEM)	TD	DEM derivatives: slope steepness, aspect, length, convexity etc.	Landslide monitoring, Change detection	Landslide monitoring, Change detection
<p>TG: too general, as the data is not sufficiently detailed for the mapping scale, TD: too detailed, and data collection too costly given the relatively low requirements at the given scale</p>					

(Source: van Westen, Cees J., Enrique Castellanos, and Sekhar L. Kuriakose. "Spatial data for landslide susceptibility, hazard, and vulnerability assessment: an overview." *Engineering geology* 102.3 (2008): 112-131)

Except from providing the necessary information to develop landslide inventories, remote sensing data can be also used for the extraction of other spatial data (environmental factors) with a crucial importance in respect to landslide susceptibility, hazard and risk assessment.

Topographic data is considered one of the major factors in landslide hazard analysis, and therefore the generation of a digital representation of the surface elevation, Digital Elevation Model (DEM), plays a major role. There are different data sources which can be used for the generation of DEMs (see table 3.3.4), but the selection depends on data availability, pricing and the targets of the research main targets.

Optical remote sensing imagery, with spatial resolution 5–15 meters (e.g. SPOT, ASTER) can be used for medium scale studies. Many derivate data can be produced from DEMs using simple GIS operations. In many landslide hazard studies include derivative data such as slope aspect in the landslide hazard analysis, although the relation between slope aspect and landslide occurrence is not always clear.

Derivatives from DEMs can be used in heuristic analysis at small scales (hillshading images for display as backdrop image, physiographic classification, internal relief,

drainage density), in statistical analysis at medium scales (e.g. altitude zones, slope gradient, slope direction, contributing area, plan curvature, profile curvature, slope length), in deterministic modelling at large scales (local drain direction, flow path, slope gradient, landslide susceptibility assessment) and in landslide run out modelling (detailed slope morphology, flow path, landslide hazard assessment, rock fall movement).

Even though there are many DEM derived data layers that can be created, are not all of them suitable for landslide susceptibility assessment and of course not applicable to all scales. As a general guideline, the use of slope gradient data layer is not advisable for small scale studies, whereas in medium scale studies slope layer, and other DEM derivatives like aspect, slope length, slope shape etc. can be used as input data for heuristic or statistical analysis.

In large and detailed scale hazard assessment, DEMs are used in slope hydrology modelling. Slope data are used for the deterministic slope stability modelling.

On the other hand, the use of high accurate DEMs (LiDAR) may cause different problems. The very high spatial resolution of Lidar data sometimes does not correspond with the detail of the rest of the data layers (ie. environmental factors etc) [62]. A brief overview of the environmental factors, which can be derived from remote sensing data and their relevance for landslide susceptibility and hazard assessment is given in the following table (Table 3.3.5).

Table 3.3.5. Environmental factors and their relevance for landslide susceptibility and hazard assessment

Group	Data layer and types	Relevance for landslide susceptibility and hazard assessment	Scale			
			Regional	Medium	Large	detailed
Digital Elevation Models	Slope gradient	Most important factor in gravitational movements	L	H	H	H
	Slope direction	Might reflect differences in soil moisture and vegetation	H	H	H	H
	Slope length/shape	Indicator for slope hydrology	H	H	H	H
	Flow direction	Used in slope	L	M	H	H

**Current Status Assessment - Investigation
on the potential use of remotely sensed data**

		hydrological modelling				
	Flow accumulation	Used in slope hydrological modelling	L	M	H	H
	Internal relief	Used in small scale assessment as indicator for type of terrain	H	M	L	L
	Drainage density	Used in small scale assessment as indicator for type of terrain	H	M	L	L
Land use	Land use map	Type of land use/land cover is a main components in stability analysis	H	H	H	H
	Land use changes	Temporal varying land use/land cover is a main components in stability analysis	M	H	H	M
H=highly applicable, M=moderately applicable, and L=Less applicable						

(Source: van Westen, Cees J., Enrique Castellanos, and Sekhar L. Kuriakose. "Spatial data for landslide susceptibility, hazard, and vulnerability assessment: an overview." *Engineering geology* 102.3 (2008): 112-131)

Another environmental factor that can be produced from remote sensing data is land use data and land use changes as well. Land cover/use changes resulting from human activities, such as deforestation, forest logging, road construction, fire and cultivation on steep slopes have a significant impact on landslide activity. Vegetation cover has effect on slope stability, on the hydrological processes of shallow landsliding (the loss of precipitation by interception, removal of soil moisture by evapotranspiration and the effects on hydraulic conductivity)

Land cover/use data can be produced with the use of medium resolution satellite imagery such as LANDSAT, SPOT, and ASTER etc. as well as multi-temporal imagery can be used for detection of the land cover/use changes. In the case of change detection, different approaches (techniques) can be performed such as post-classification comparison, temporal image differencing, temporal image rationing, or Bayesian probabilistic methods.

4 REMOTE SENSING IN THE PROJECT’S FRAMEWORK

The investigation of the use of remote sensing in the project’s framework was based on the data availability in terms of acquisition cost, the proposed scales of analysis, and the easiness of methods.

As it presented previously (chapter 2) nowadays there are different remote sensing data which can be exploited for the natural hazard studies. The key issue is what kind of imagery data can be used in the context of project requirements. In the following table (Table 4.1) is presented the EO data availability (without purchase cost) in conjunction with their applicability to the different scales of analysis and the techniques that can be performed (easiness of application).

Landsat TM and ETM+ satellite data were used in the landslide hazard assessment procedures in the SciNetNatHaz project. This type of data is freely available from the NASA Landsat program:

(<http://glcf.umd.edu/data/landsat/> and <http://earthexplorer.usgs.gov/>).

Open Source and freeware software was used for the entire processing and interpretation phases: Multispec[®] (Biehl & Landgrebe, Purdue University, USA) and GRASS GIS[®]. Data and information produced were incorporated into a Geographic Information System developed with Quantum GIS (QGIS).

Table 4.1 overview of EO data availability and their applicability

EO Data	Type	Application	Parameter	Technique	Description	Easiness of application	Scale	
							Regional	Local
Optical Satellite images	Landsat TM 4-5 Landsat 8	Floods	flood depth	Spectra enhancement (e.g. PCA)	Estimation of flood depth from past flood events	N	H	L
			Land cover	Supervised image classification	update land cover maps in order to produce Manning roughness factor map	X	H	M

Current Status Assessment - Investigation on the potential use of remotely sensed data

DEM	ASTER (25m), global coverage		flood depth	Topographic Wetness Index (TWI)	Using GIS processes	Y	H	L
Optical Satellite images	Landsat TM 4-5 Landsat 8	Landslides	Landslides inventory	Image rationing, thresholding, Single data images, with pixel based image classification	Mapping landslides	X	H	M
			Environmental factors	Multiple date images, with pixel based image classification	Mapping/update land use/cover, Land cover/use change detection	X	H	H
DEM	ASTER (25m), global coverage		DEM derivatives (Environmental factors)	GIS processes	DEM derivatives: slope steepness, aspect, length, convexity etc.	Y	H	L
Easiness of application: Y=easy, X=moderate, N=not easy, Applicable: H=highly applicable, M=moderately applicable, and L=Less applicable								

4.1 REMOTE SENSING ANALYSIS TO IMPROVE LANDSLIDE HAZARD ASSESSMENT PERFORMANCE

4.1.1 Introduction – Scope

Landslide Hazard Assessment on a regional scale can provide useful information which when combined with a preliminary risk assessment can support decision regarding strategic planning for disaster prevention. Such a strategic planning can

*Current Status Assessment - Investigation
on the potential use of remotely sensed data*

provide the State Regional and local administration with the tool to effectively plan Landslide disaster mitigation measures in both their financial and technical aspects.

In this aspect, important questions arising are related to the reliability and accuracy of the assessments since decisions have to be made and money and effort spent.

Effective strategic planning landslide disaster mitigation measures requires an, as accurate as possible, landslide hazard assessment.

Engineering geology and geotechnical engineering research and practical experience has provided the background for the development of various landslide assessment methodologies, including the ones used in this project.

As already presented in previous other SciNetNatHaz project documents (D.1.02, D.03.01) the project partners have decided to test different methodological approaches in order to select one that is feasible to implement under the current circumstances and that can provide quality, harmonized results.

In respect to the quality of results, two main aspects are taken into consideration: i) reliability, which concerns the “reliable” definition of areas of high degree of Landslide Hazard and ii) accuracy, which concerns the degree of locating those “high” hazard areas.

Since all Hazard Assessment methodologies include a degree of uncertainty, the project partners have selected three very well known, scientifically sound and worldwide used landslide hazard assessment methodologies: Mora & Vahrson, FEMA methodology (HazUS) and the calculation of the Factor of Safety.

As all of the available LHA methodologies, these three take into consideration the engineering properties of geologic formations which are not uniform throughout large areas.

In fact, engineering properties vary very much even in small areas due to stresses and strains which have affected the geologic formations in their past. This effect reaches its highest level when dealing with fractured zones within rock formations because rock materials usually present medium to good engineering properties when intact and extremely poor when fractured; the degradation being a function of fracture intensity and erosion degree. Fracture zones are permeable zones where water accumulates especially during rainfall events, further decreasing the already poor engineering properties and the respective geotechnical behavior of these zones. Erosion also progresses faster in those zones due to the moisture present and to the volume of rock particles thus further degrading the engineering properties of the material.

*Current Status Assessment - Investigation
on the potential use of remotely sensed data*

As is evident, the presence of such zones within a hard geologic formation must be taken into consideration otherwise the LHA outputs, no matter the methodology used, will be poorly related to actual conditions.

For that reason effort has been spent to detect and map such features in order to incorporate their effect into the engineering properties of rocks and thus to include them in the related to LHA calculations.

Mapping those tectonic features in the field is very difficult even when working in large scale projects (1/5.000 or larger) due to the presence of high vegetation and also to their scale because they usually have lengths of kilometers and width of tens of meters.

Remote Sensing on the other hand can provide in this case the solution, as has been shown by pervious research [66], [67].

Remote Sensing techniques and Landsat TM and ETM+ data were used in order to detect and map lineaments and to define tectonic features.

The outputs were then incorporated into the evaluation of the engineering properties of geologic formations and in the LHA calculations. Landslide Hazard Assessment (LHA) outputs were compared to field observations especially on cut slopes where a clear picture of the geologic structure was displayed.

Test area for this research was the area of Nymfaia-Greek/Bulgarian border road where numerous high cut slopes with stability problems exist. Within this context, cut slopes as high as 50m were observed along the Nymfaia-Bulgarian border road axis.

As resulted, the LHA outputs after the incorporation of remotely sensed fractures, improved significantly providing extremely close estimations to actual events investigated in situ.

4.1.2 Materials and Data

Rocks outcropping in Serres and Nymfaia area appear to be badly fractured. The spatial distribution of the degree/density rocks in the area are fractured, varies greatly within these areas, making the reliable and accurate evaluation of the mechanical characteristics of the geological formations very difficult.

Weathering is another process that plays an important role in the geotechnical behavior of the geologic formations and weathering processes are also greatly affected by fracturing.

Inability to better define those factors renders any attempt to assess landslide hazard on a regional scale and provide accurate and reliable results, almost impossible. For

*Current Status Assessment - Investigation
on the potential use of remotely sensed data*

those reasons, any assessment attempted may be from very accurate in the case of no fractured zones present in rocks, to very inaccurate in the opposite case.

Geologic maps were used to map faults in the aforementioned areas. Geologic maps were compiled 30-40 years ago so these maps are mostly based on ground observations and on examining aerial photographs.

For that reason, geologic maps only contain a small number of faults mainly due to the fact that these maps were produced before 1980 when no contemporary technologies were widely used; so they represent a small number of the actual existing fractures in the areas.

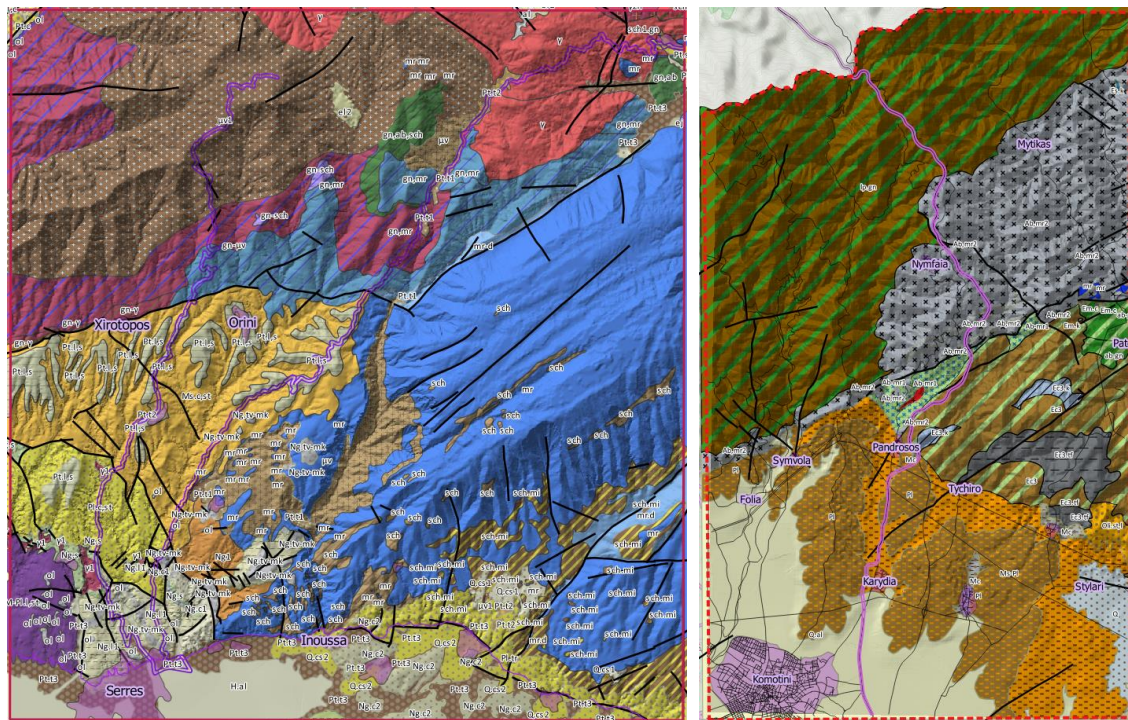


Fig4. Geologic Maps and Tectonic regime of Serres (left) and Nymfaia (right) pilot implementation areas. Fault traces digitized from Geologic Maps produced by the Institute of Geological & Mineral Exploration, Greece.

Data used included digitized topographic maps 1:50.000 scale; Landsat TM images and Landsat ETM+ images.

Freely available software was used including Multispec© for remote sensing applications and Quantum GIS (QGIS).

*Current Status Assessment - Investigation
on the potential use of remotely sensed data*

Hardware used included a high power Toshiba (Qosmio) laptop and for the in situ investigations, a field data collection device (suitable for fieldwork tablet; waterproof and dustproof, running on ANDROID OS).

The aim of this process was not just to detect lineaments but to detect lineaments that most likely correspond to fractured zones so processing and interpretation of Remote Sensing data focused on producing the respective outputs.

To that end, selection of Landsat TM and ETM bands and the creation of band ratios was based on the “physical meaning” of the possible band combinations. “Physical Meaning” as a term used herein means the relation between actual geological features, and the recorded spectra due to their influence on the incident electromagnetic radiation which is reflected, refracted or absorbed.

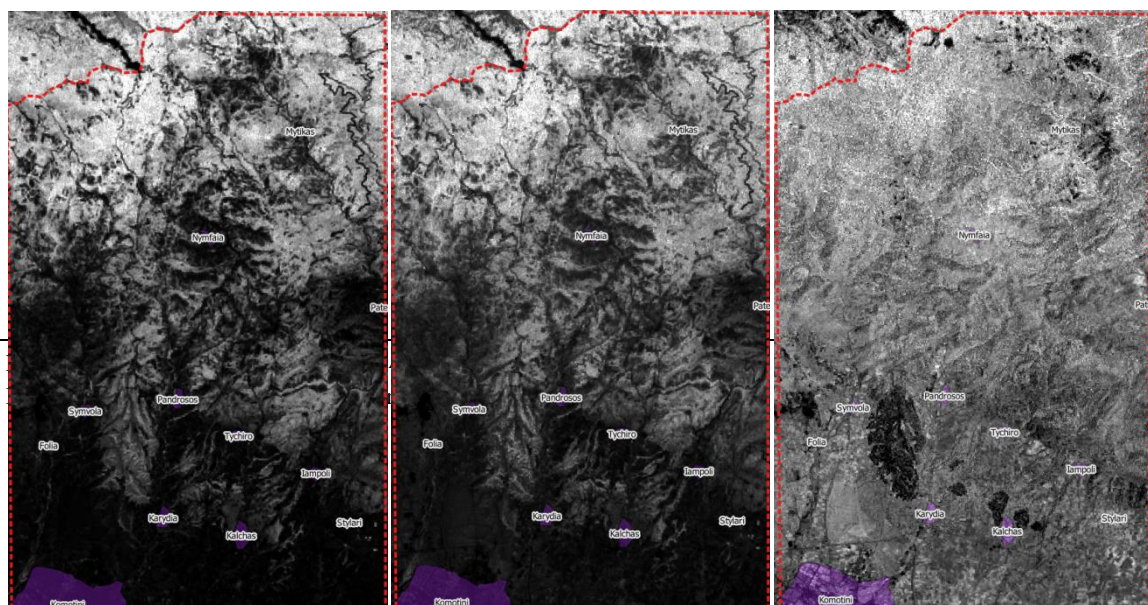
As already stated, fractured zones in geologic formations are related to the presence of loose rock, very erodible and also to the presence of near-surface water. These assumptions lead to the conclusion that intense erosion in fractured zones has led to the development of a thick soil layer; which is actually a fact. A thicker, as compared to the rest of the area, soil layer combined with the favorable presence of water in those zones, promotes the development of vegetation so, more dense and more vigorous vegetation exists in fractured zones than in their surroundings.

Landsat TM and ETM+ images were used for this investigation.

For the reasons mentioned above, Landsat TM and ETM+ bands including NIR (TM4) and SWIR (TM5) for vegetation and TM3 (RED) as a contrast to them (minimum vegetation reflectance) were selected.

An additional factor taken into consideration was the presence of higher moisture content in fractured zones, so Landsat bands including SWIR2 (TM7) in combination with bands TM1 (BLUE) and TM3 (RED) were also used.

Remote Sensing data processing included the creation of the multispectral image of the wider area, band ratios enhancing the features under investigation, false color composites (FCC) and visual analysis and interpretation.

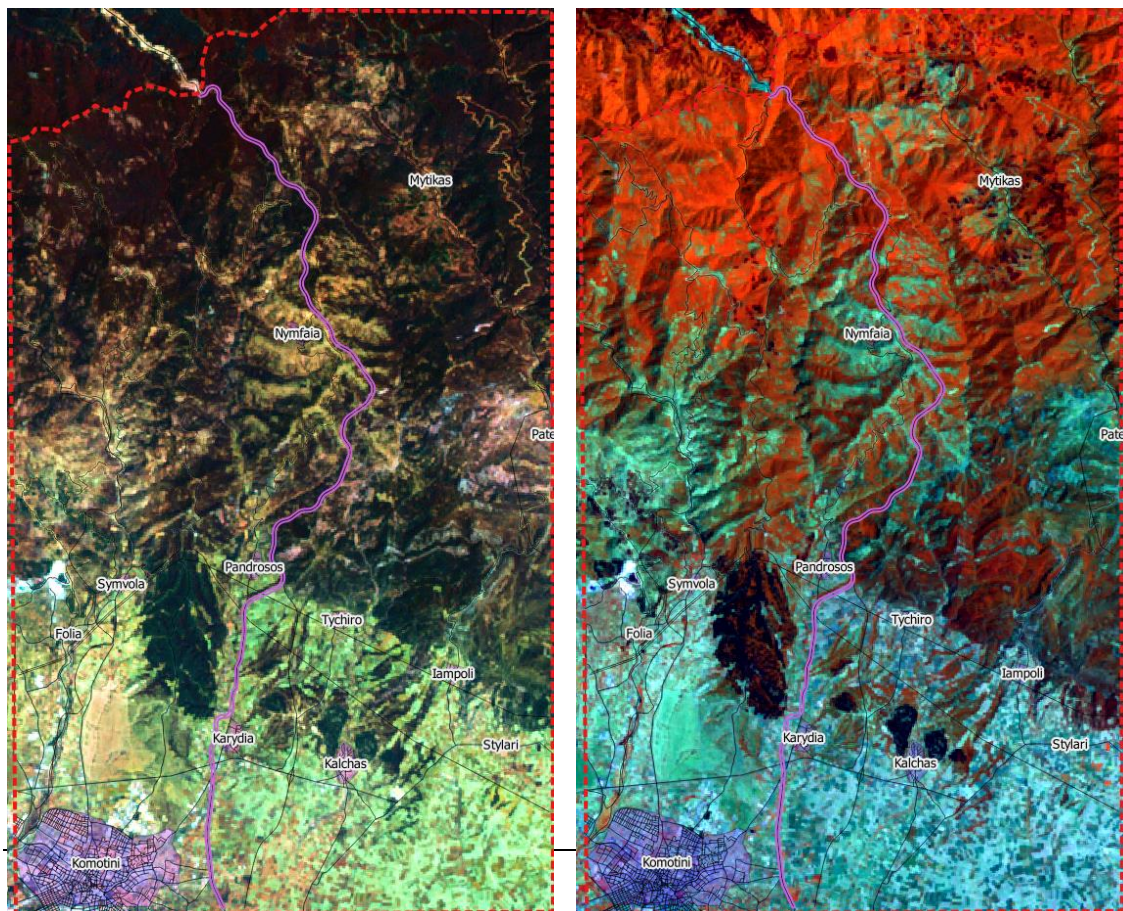


*Current Status Assessment - Investigation
on the potential use of remotely sensed data*

Fig. 5 Nymfaia pilot implementation area. Band Ratios –Inversed images (left to right): TM4/TM3, TM5/TM3, TM7/TM3, showing large lineaments (center) with WSW-ENE; SW-NE and NW-SE directions. Landsat TM and ETM+ data (NASA) were downloaded from <http://glcf.umd.edu/data/landsat/> .

As resulted, band ratio TM4/TM3, also considered as a “vegetation index”, provided a lot of valuable information regarding linear features corresponding to higher reflectance values or more dense and/or vigorous vegetation.

Please note that images in Fig. 6 are inversed to show the lineaments as black lines which show better in printed material.



*Current Status Assessment - Investigation
on the potential use of remotely sensed data*

Fig6. False Color Composites (FCC): TM7-TM3-TM1 (left) and TM4-TM5-TM3 (right) used to trace lineaments and map fractured zones in rocks (Nymfaia PIA).

Based on the interpretation of the remote sensing processing outputs, a number of 410 fractures were mapped for the Serres PIA area (500km²) and 232 for Nymfaia area (200km²) as shown in Fig 7.

At a next step, 30m buffer zones (total width) were created around these features, corresponding to areas influenced by fracturing. These areas possess lower engineering properties as has been described in previous paragraphs; a fact taken into consideration for adapting to local conditions the various methodologies adopted, in order to assess Landslide Hazard in the pilot implementation areas.

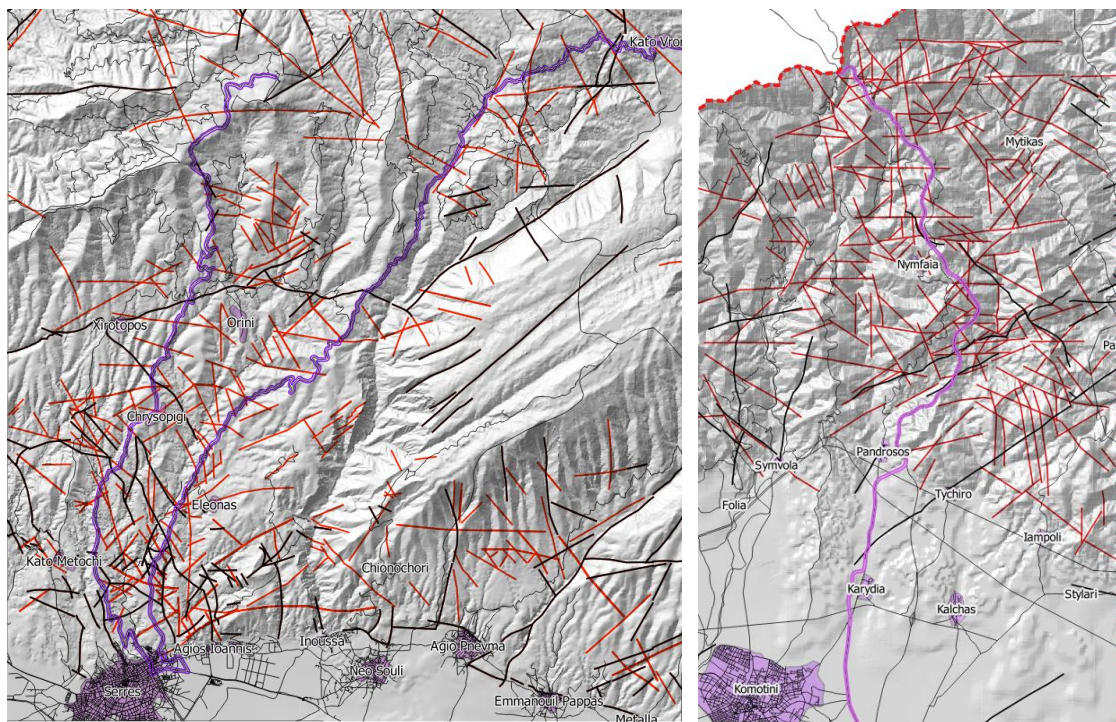


Fig7. Tectonic regime of Serres and Nymfaia pilot implementation areas. Major road axes in both areas shown in purple. Fault traces digitized from Geologic Maps (black lines) and fractures mapped using Remote Sensing techniques (red lines). (Geologic Maps produced by the Institute of Geological & Mineral Exploration, Greece).

5 REFERENCES

- [1] Joyce, Karen E., et al. "A review of the status of satellite remote sensing and image processing techniques for mapping natural hazards and disasters." *Progress in Physical Geography* 33.2 (2009): 183-207.
- [2] Gillespie, Thomas W., et al. "Assessment and prediction of natural hazards from satellite imagery." *Progress in Physical Geography* 31.5 (2007): 459-470.
- [3] Evangelidis, Konstantinos, et al. "Geospatial services in the Cloud." *Computers & Geosciences* 63 (2014): 116-122.
- [4] Chiroiu, L., and G. Andre. "Damage assessment using high resolution satellite imagery: Application to 2001 Bhuj, India, earthquake." Proc. 7th National Conference on Earthquake Engineering. 2001.
- [5] Saito, Keiko, et al. "Using high-resolution satellite images for post-earthquake building damage assessment: a study following the 26 January 2001 Gujarat earthquake." *Earthquake Spectra* 20.1 (2004): 145-169.
- [6] Yamazaki, Fumio, et al. "Earthquake damage detection using high-resolution satellite images." *Geoscience and Remote Sensing Symposium, 2004. IGARSS'04. Proceedings. 2004 IEEE International. Vol. 4. IEEE, 2004.*
- [7] Dong, Laigen, and Jie Shan. "A comprehensive review of earthquake-induced building damage detection with remote sensing techniques." *ISPRS Journal of Photogrammetry and Remote Sensing* 84 (2013): 85-99.
- [8] Saito, K., Spence, R.J.S., 2005. Visual damage assessment using high-resolution satellite images following the 2003 Bam, Iran, earthquake. *Earthquake Spectra* 21 (S1), S309–S318.
- [9] Yamazaki, F., Y. Yano, M. Matsuoka., 2005. Visual damage interpretation of buildings in Bam city using QuickBird images following the 2003 Bam, Iran earthquake. *Earthquake Spectra*, 21(S1): 329–336.
- [10] Stramondo, S., et al. "Satellite radar and optical remote sensing for earthquake damage detection: results from different case studies." *International Journal of Remote Sensing* 27.20 (2006): 4433-4447.
- [11] Yusuf, Y., Matsuoka, M., Yamazaki, F., 2001. "Damage assessment after 2001 Gujarat earthquake using Landsat-7 satellite images." *Journal of the Indian Society of Remote Sensing* 29 (1), 233–239.

- [12] Zhang, Jing-Fa, Li-li Xie, and Xia-xin Tao. "Change detection of earthquake-damaged buildings on remote sensing image and its application in seismic disaster assessment." *Geoscience and Remote Sensing Symposium, 2003. IGARSS'03. Proceedings. 2003 IEEE International. Vol. 4. IEEE, 2003.*
- [13] Rathje, E.M.; Kyu-Seok Woo; Crawford, M.; Neuenschwander, A., "Earthquake damage identification using multi-temporal high-resolution optical satellite imagery," In: *IEEE International Geoscience and Remote Sensing Symposium 2005*, vol. 7, pp. 5045–5048.
- [14] Tomowski, D., et al. "Change visualization through a texture-based analysis approach for disaster applications." *ISPRS Technical Commission VII Symposium—100 Years ISPRS Advancing Remote Sensing Science. Vol. 38. Vienna University of Technology, Austria, 2010.*
- [15] Tralli, David M., et al. "Satellite remote sensing of earthquake, volcano, flood, landslide and coastal inundation hazards." *ISPRS Journal of Photogrammetry and Remote Sensing* 59.4 (2005): 185-198..
- [16] Bitelli, G., et al. "Image change detection on urban area: the earthquake case." *XXth ISPRS Congress, Istanbul, Turkey. 2004.*
- [17] Gusella, Luca, et al. "Object-oriented image understanding and post-earthquake damage assessment for the 2003 Bam, Iran, earthquake." *Earthquake Spectra* 21.S1 (2005): 225-238.
- [18] Li, Peijun, et al. "Urban building damage detection from very high resolution imagery using one-class SVM and spatial relations." *Geoscience and Remote Sensing Symposium, 2009 IEEE International, IGARSS 2009. Vol. 5. IEEE, 2009.*
- [19] Matsuoka, Masashi, and Fumio Yamazaki. "Use of satellite SAR intensity imagery for detecting building areas damaged due to earthquakes." *Earthquake Spectra* 20.3 (2004): 975-994.
- [20] Chini, M., et al. "Uplift and subsidence due to the 26 December 2004 Indonesian earthquake detected by SAR data." *International Journal of Remote Sensing* 29.13 (2008): 3891-3910.
- [21] Wang, Haipeng, and Ya-Qiu Jin. "Statistical analysis to assess building damage in 2008 Wenchuan earthquake from multi-temporal SAR images." *Synthetic Aperture Radar, 2009. APSAR 2009. 2nd Asian-Pacific Conference on. IEEE, 2009.*
- [22] Ito, Yosuke, et al. "Extraction of damaged regions using SAR data and neural networks." *International Archives of Photogrammetry and Remote Sensing* 33.B1; PART 1 (2000): 156-163.

- [23] Matsuoka, Masashi, and Fumio Yamazaki. "Use of interferometric satellite SAR for earthquake damage detection." *In: Proceedings of 6th International Conference of Seismic Zonation*; (2000):103–108.
- [24] Hoffmann, J. "Mapping damage during the Bam (Iran) earthquake using interferometric coherence." *International Journal of Remote Sensing* 28.6 (2007): 1199-1216.
- [25] Yonezawa, C., and S. Takeuchi. "Decorrelation of SAR data by urban damages caused by the 1995 Hyogoken-nanbu earthquake." *International Journal of Remote Sensing* 22.8 (2001): 1585-1600.
- [26] Chini, Marco, Nazzareno Pierdicca, and William J. Emery. "Exploiting SAR and VHR optical images to quantify damage caused by the 2003 Bam earthquake." *Geoscience and Remote Sensing, IEEE Transactions on* 47.1 (2009): 145-152.
- [27] Dell'Acqua, Fabio, et al. "Earthquake damages rapid mapping by satellite remote sensing data: L'Aquila april 6th, 2009 event." *Selected Topics in Applied Earth Observations and Remote Sensing, IEEE Journal of* 4.4 (2011): 935-943.
- [28] Walker, Richard Thomas. "A remote sensing study of active folding and faulting in southern Kerman province, SE Iran." *Journal of Structural Geology* 28.4 (2006): 654-668.
- [29] Fu, Bihong, et al. "Mapping active fault associated with the 2003 Mw 6.6 Bam (SE Iran) earthquake with ASTER 3D images." *Remote Sensing of Environment* 92.2 (2004): 153-157.
- [30] Mah, Abdullah, et al. "Lineament analysis of Landsat Thematic Mapper images, Northern Territory, Australia." *Photogrammetric engineering and remote sensing* 61.6 (1995): 761-773.
- [31] Philip, G. "Landsat Thematic Mapper data analysis for Quaternary tectonics in parts of the Doon valley, NW Himalaya, India." *International Journal of Remote Sensing* 17.1 (1996): 143-153.
- [32] Suzen, M. L., and V. Toprak. "Filtering of satellite images in geological lineament analyses: an application to a fault zone in Central Turkey." *International Journal of Remote Sensing* 19.6 (1998): 1101-1114.
- [33] Schumann, Guy, et al. "Progress in integration of remote sensing–derived flood extent and stage data and hydraulic models." *Reviews of Geophysics* 47.4 (2009).

- [34] Sandholt, Inge, et al. "Remote sensing techniques for flood monitoring in the Senegal River Valley." *Geografisk Tidsskrift-Danish Journal of Geography* 103.1 (2003): 71-81.
- [35] Wang, Y., J. D. Colby, and K. A. Mulcahy. "An efficient method for mapping flood extent in a coastal floodplain using Landsat TM and DEM data." *International Journal of Remote Sensing* 23.18 (2002): 3681-3696.
- [36] Barton, Ian J., and Janice M. Bathols. "Monitoring floods with AVHRR." *Remote Sensing of Environment* 30.1 (1989): 89-94.
- [37] Sanyal, Joy, and X. X. Lu. "Application of remote sensing in flood management with special reference to monsoon Asia: a review." *Natural Hazards* 33.2 (2004): 283-301.
- [38] McFeeters, S. K. "The use of the Normalized Difference Water Index (NDWI) in the delineation of open water features." *International journal of remote sensing* 17.7 (1996): 1425-1432.
- [39] Xu, Hanqiu. "Modification of normalised difference water index (NDWI) to enhance open water features in remotely sensed imagery." *International Journal of Remote Sensing* 27.14 (2006): 3025-3033.
- [40] TEWARI, S., et al. "Remote monitoring of forest response to changed soil moisture regime due to river regulation." *J. FOR. SCI* 49.9 (2003): 429-438.
- [41] Ghorbanali, A., and N. Nouri. "Coastline change detection using remote sensing." *International Journal of Environmental Science & Technology* 4.1 (2007): 61-66.
- [42] Wang, Y., J. D. Colby, and K. A. Mulcahy. "An efficient method for mapping flood extent in a coastal floodplain using Landsat TM and DEM data." *International Journal of Remote Sensing* 23.18 (2002): 3681-3696.
- [43] Jain, Sanjay K., et al. "Delineation of flood-prone areas using remote sensing techniques." *Water Resources Management* 19.4 (2005): 333-347.
- [44] Qing, Yang Cunjian Zhou Chenghu Wan. "Deciding the flood extent with Radarsat SAR data and Image Fusion." *ACRS*, 1999.
- [45] Islam, M. M., and Sado, K. "Flood damage and management modelling using satellite remote sensing data with GIS: case study of Bangladesh." *Remote sensing and hydrology 2000. Selected papers from a conference held at Santa Fe, New Mexico, USA, 2-7 April 2000.* IAHS Press, 2001.

- [46] Sanyal, Joy, and X. X. Lu. "Remote sensing and GIS-based flood vulnerability assessment of human settlements: a case study of Gangetic West Bengal, India." *Hydrological Processes* 19.18 (2005): 3699-3716.
- [47] Geudtner, D., R. Winter, and P. W. Vachon. "Flood monitoring using ERS-1 SAR interferometry coherence maps." *Geoscience and Remote Sensing Symposium, 1996. IGARSS'96. Remote Sensing for a Sustainable Future.*, International. Vol. 2. IEEE, 1996.
- [48] Townsend, Philip A., and Stephen J. Walsh. "Modeling floodplain inundation using an integrated GIS with radar and optical remote sensing." *Geomorphology* 21.3 (1998): 295-312.
- [49] Beven, K. J., and M. J. Kirkby. "A physically based, variable contributing area model of basin hydrology." *Hydrological Sciences Journal* 24.1 (1979): 43-69.
- [50] Versini, P-A., Eric Gaume, and Herve Andrieu. "Assessment of the susceptibility of roads to flooding based on geographical information—test in a flash flood prone area (the Gard region, France)." *Natural Hazards and Earth System Science* 10.4 (2010): 793-803.
- [51] Manfreda, Salvatore, Margherita Di Leo, and Aurelia Sole. "Detection of flood-prone areas using digital elevation models." *Journal of Hydrologic Engineering* 16.10 (2011): 781-790.
- [52] Van der Sande, C. J., S. M. De Jong, and A. P. J. De Roo. "A segmentation and classification approach of IKONOS-2 imagery for land cover mapping to assist flood risk and flood damage assessment." *International Journal of Applied Earth Observation and Geoinformation* 4.3 (2003): 217-229.
- [53] Pradhan, Biswajeet. "Flood susceptible mapping and risk area delineation using logistic regression, GIS and remote sensing." *Journal of spatial hydrology* 9.2 (2010).
- [54] Gashaw, Woubet, and Dagnachew Legesse. "Flood Hazard and Risk Assessment Using GIS and Remote Sensing in Fogera Woreda, Northwest Ethiopia." *Nile River Basin*. Springer Netherlands, 2011. 179-206.
- [55] Khan, Sadiq I., et al. "Satellite remote sensing and hydrologic modeling for flood inundation mapping in Lake Victoria Basin: Implications for hydrologic prediction in ungauged basins." *Geoscience and Remote Sensing, IEEE Transactions on* 49.1 (2011): 85-95.
- [56] Domeneghetti, Alessio, et al. "The use of remote sensing-derived water surface data for hydraulic model calibration." *Remote Sensing of Environment* 149 (2014): 130-141.

[57] Mantovani, Franco, Robert Soeters, and C. J. Van Westen. "Remote sensing techniques for landslide studies and hazard zonation in Europe." *Geomorphology* 15.3 (1996): 213-225.

[58] Soeters, R., and C. J. van Westen. "Slope Instability Recognition, Analysis and Zonation" in Turner, A.K and Schuster, R.L., (Eds): *Landslides: Investigation and mitigation*. Transportation Research Board, Special Report 247. Washington, DC: National Academy Press (1996).

[59] Tofani, V., et al. "Technical note: use of remote sensing for landslide studies in Europe." *Natural Hazards and Earth System Science* 13.2 (2013): 299-309.

[60] Nichol, J., and M. S. Wong. "Satellite remote sensing for detailed landslide inventories using change detection and image fusion." *International Journal of Remote Sensing* 26.9 (2005): 1913-1926.

[61] Nichol, Janet E., Ahmed Shaker, and Man-Sing Wong. "Application of high-resolution stereo satellite images to detailed landslide hazard assessment." *Geomorphology* 76.1 (2006): 68-75.

[62] van Westen, Cees J., Enrique Castellanos, and Sekhar L. Kuriakose. "Spatial data for landslide susceptibility, hazard, and vulnerability assessment: an overview." *Engineering geology* 102.3 (2008): 112-131.

[63] Cheng, K. S., C. Wei, and S. C. Chang. "Locating landslides using multi-temporal satellite images." *Advances in Space Research* 33.3 (2004): 296-301.

[64] Dymond, John R., et al. "Validation of a region-wide model of landslide susceptibility in the Manawatu–Wanganui region of New Zealand." *Geomorphology* 74.1 (2006): 70-79.

[65] Joyce, K. E., G. D. Dellow, and Phil J. Glassey. "Assessing image processing techniques for mapping landslides." *Geoscience and Remote Sensing Symposium, 2008. IGARSS 2008. IEEE International*. Vol. 2. IEEE, 2008.

[66] Papatheodorou C. "GroundWater flow paths delineation using Remote Sensing techniques and GIS". 30th EARSel Symposium, Remote Sensing for Science, Education, Natural and Cultural Heritage, Paris, France, June 2010.

[67] Papatheodorou C., et.al. "A Remotely Sensed contribution to the Western Attica (Greece) tectonic Geology. 32nd EARSel Symposium and 36th General Assembly. Mykonos Island, Greece 21st - 24th May 2012.



6 ANNEX I – SATELLITE SENSORS

Table 2.1. Summary of the characteristics of some commercial satellite sensors

Satellite	Launch (year)	Sensor	Swath (Km)	Nadir Spatial Resolution (m)	Spectral bands	Revisit capability	Stereo Imagery
ALOS	2006	AVNIR-2	35	10	B1:Blue, B2:Green, B3:Red, B4:NIR	46 days	No
		PRISM	35	2,5	B1:Panchromatic		Yes
DubaiSat-1	2009	Panchromatic	20	2,5	B1:Panchromatic, B2:Blue, B3:Green, B4:Red, B5:NIR		No
		Multispectral	20	5			
EnviSAT	2002	Meris	1150	300	VIS-NIR: 15 bands selectable across range: 390 nm to 1040 nm	3 days	No
EO-1	2000	ALI	185	30	B1:Panchromatic, B2:Blue 1, B3:Blue 2, B4:Green, B5:Red, B6:NIR 1, B7:NIR 2, B8:MIR 1, B9:MIR 2, B10:MIR 3	30 days	No



*Current Status Assessment - Investigation
on the potential use of remotely sensed data*

		Hyperion	7,5	30	hyperspectral (400- 2500nm),		
EROS-A	2000	PIC	12,5	1,8	Panchromatic	-	Yes
EROS-B	2006	PIC 2	13,5	0,7	Panchromatic	-	Yes
GeoEye 1	2008	Panchromatic	15,2	0,41		2,8 days	Yes
		Multispectral	15,2	1,64	B1:Panchromatic, B2:Blue, B3:Green, B4:Red, B5:NIR		
Formosat 2	2004	Panchromatic	24	2		1 day	Yes
		Multispectral	24	8	B1:Blue, B2:Green, B3:Red, B4:NIR, B5:Panchromatic		
IKONOS	1999	Panchromatic	11,3	0,82		3 days	Yes
		Multispectral	11,3	3,2	B1:Panchromatic, B2:Blue, B3:Green, B4:Red, B5:NIR		
IRS-P5	2005	Panchromatic	30	2,5	B1:Panchromatic 1, B2:Panchromatic 2	5 days	No
IRS-P6	2003	LISS-3	140	23,5	B1:Green, B2:Red, B3:NIR, B4:MIR	5 days	Yes
		LISS-4	23,9 and 70	5,8	B1:Green, B2:Red, B3:NIR, B4:Monochromatic		
		AWiFS	740	56	B1:Green, B2:Red, B3:NIR, B4:MIR		No
Kompsat 2	2006	MSC	15	4	B1:Panchromatic, B2:Blue, B3:Green, B4:Red, B5:NIR		No



*Current Status Assessment - Investigation
on the potential use of remotely sensed data*

Kompsat 3	2012	Panchromatic	16,8	0,7			No
		AEISS	16,8	2,8	B1:Panchromatic, B2:Blue, B3:Green, B4:Red, B5:NIR		
Landsat 4	1982	TM	185	30-120	B1:Blue, B2:Green, B3:Red, B4:Near Infrared, B5:Mid Infrared 1, B6:Thermal, B7:Mid Infrared 2	28 days	No
Landsat 5	1984	TM	185	30-120	B1:Blue, B2:Green, B3:Red, B4:Near Infrared, B5:Mid Infrared 1, B6:Thermal, B7:Mid Infrared 2	16 days	No
Landsat 7	1999	ETM+ Panchromatic	185	15		16 days	No
		ETM+ Multispectral	185	30	B1:Blue, B2:Green, B3:Red, B4:Near Infrared, B5:Mid Infrared 1, B6:Thermal, B7:Mid Infrared 2, B8:Panchromatic		
		ETM+ Thermal	185	60			
Landsat 8	2013	OLI	185	30 (B8 15)	B1:Coastal Aerosol, B2:Blue, B3:Green, B4:Red, B5:NIR, B6:MIR 1, B7:MIR 2, B8:Panchromatic, B9:Cirrus, B10:Thermal 1, B11:Thermal 2	16 days	No
		TIRS	185	120			
NigeriaSat X	2011	SLIM 6	660	22	B1:Green, B2:Red, B3:NIR		No
NigeriaSat - 2	2011	Panchromatic	20	2,5		1 day	No
		VHRI	20	5	B1:Blue, B2:Green, B3:Red, B4:NIR, B5:Panchromatic		
		MRI	500	32	B1:Blue, B2:Green, B3:Red, B4:NIR		



*Current Status Assessment - Investigation
on the potential use of remotely sensed data*

OrbView-3	2003	Panchromatic	8	1	B1:Panchromatic, B2:Blue, B3:Green, B4:Red, B5:NIR	3 days	Yes
		Multispectral	8	4			
Pleiades-1A	2011	Panchromatic	20	0,5	B1:Panchromatic, B2:Blue, B3:Green, B4:Red, B5:NIR	1 day	Yes
		Multispectral	20	2			
Pleiades-1B	2012	Panchromatic	20	0,5	B1:Panchromatic, B2:Blue, B3:Green, B4:Red, B5:NIR	1 day	Yes
		Multispectral	20	2			
Proba	2001	Chris	14	18	hyperspectral	7 days	Yes
QuickBird	2001	Panchromatic	16,5	0,61	B1:Panchromatic, B2:Blue, B3:Green, B4:Red, B5:NIR	1-3,5 days	Yes
		Multispectral	16,5	2,44			
RapidEye	2008	Multispectral	78	6,5	B1:Blue, B2:Green, B3:Red, B4:Red Edge, B5:NIR	1 day	No
Resurs-DK1	2006	Panchromatic	28	0,8	B1:Panchromatic, B2:Blue, B3:Green, B4:Red, B5:NIR		No
		Multispectral	28	2,5			
RazakSat	2007	Panchromatic	20	2,5	B1:Panchromatic, B2:Blue, B3:Green, B4:Red, B5:NIR		No
		Multispectral	20	5			
SPOT-4	1998	Panchromatic	60–80	10	B1:Green, B2:Red, B3:Near, Infrared,	11 times every	Yes



*Current Status Assessment - Investigation
on the potential use of remotely sensed data*

		Multispectral	60–80	20	B4:Mid Infrared	26 days	No
SPOT-5	2002	Panchromatic	60–80	5	B1:Green, B2:Red, B3:Near, Infrared, B4:Mid Infrared, B5:Panchromatic 1, B6:Panchromatic 2	11 times every 26 days	Yes
		Multispectral	60–80	10			
SPOT-6 - SPOT-7	2012	Panchromatic	60	1,5	B1:Panchromatic, B2:Blue, B3:Green, B4:Red, B5:NIR	1 day	Yes
		Multispectral	60	6			
Terra	1999	Modis	2330	250-500- 1000	B1-B2:Land/Clouds/Aerosol/Boundaries, B3-B7:Land/Clouds/Aerosol/Properties, B8-B16:Ocean Color/Phytoplankton/Biogeochemistry, B17-B19:Atmospheric Water Vapor, B20- B23:Surface/Cloud Tmperature, B24- B25:Atmospheric Temperature, B26- B28:Cirus Clouds-Water Vapor, B29:Cloud Properties, B30:Ozone, B31- B32:Surface/Cloud Temperature, B33- B36:Cloud Top Altitude	16 days	No
		Aster	60	15-30-90	B1:Green, B2:Red, B3:NIR, B3b:NIR Backwards, B4-B9:SWIR, B10-B14: Thermal	16 days	Yes
TopSat	2005	Panchromatic	15	2,5	B1:Panchromatic, B2:Blue, B3:Green, B4:Red	6 days	No
		Multispectral	10	5			



*Current Status Assessment - Investigation
on the potential use of remotely sensed data*

UK-DMC - 2	2009	Multispectral Camera UK- DMC2	650	20	B1:Green, B2:Red, B3:NIR		No
Worldview-1	2007	Panchromatic	17,6	0,5	B1:Panchromatic	1,7 days	Yes
Worldview-2	2009	Panchromatic	16,4	0,46	B1:Panchromatic, B2:Coastal Blue, B3:Blue, B4:Green, B5:Yellow, B6:Red, B7:Red Edge, B8:NIR 1, B9:NIR 2	1,1 days	No
		Multispectral	16,4	1,8			
Worldview-3	2014	Panchromatic	13,1	0,31		1 day	No
		Multispectral	13,1	1,24	Panchromatic, Red, Red Edge, Coastal, Blue, Yellow, NIR 1, NIR 2		
		Short Wave Infrared	13,1	3,7	8 SWIR: 1195 nm - 2365 nm		
		CAVIS	13,1	30	Desert Clouds, Aerosol-1, Aerosol-2, Aerosol- 3, Green, Water-1, Water- 2, Water-3, NDVI-SWIR, Cirrus, Snow		



Table 2.2. Utility of sensors used for mapping and monitoring different hazard types

Spectral	Visible – NIR				SWIR			Hyperspectral		Thermal		SAR		LiDAR	
	Very high	High	Medium	Coarse	High	Medium	Coarse	Very high	Medium	Medium	Coarse	polarization	Polarimetric	DEM	
Spatial (very high = <5 m, high = 5–20 m, medium = 20–250 m, coarse = >250 m)															
Sensor example	Quickbird, Ikonos	SPOT	Landsat	MODIS	ASTER	Landsat	MODIS	CASI	Hyperion	Landsat	MODIS	Radarsat-1	Terra	Airborne Sensor	
							AVHRR	Hymap					SAR-X		
	Fault location	B	C	C	E	C	C	E	B	C	E	E	B	E	A
Earthquakes	Deformation	E	E	E	E	E	E	E	E	E	E	E	A	C	A



Landslides	Scar + debris flow	B	A	B	C	E	E	E	B	B	E	E	C	D	B
	Isolate scar from debris flow	C	C	E	E	E	E	E	C	C	E	E	C	D	B
Flooding	Inundated area	A	A	B	C	B	B	C	B	B	B	C	A	A	B
	building and property damage	A	B	B	C	C	C	E	B	B	E	E	C	D	C

A: Clearly demonstrated to work using standard image processing systems and is openly available in the literature

B: Shown to work with experimental image data sets or over limited area with very small pixels or over global scales with large pixels

C: If extent is bigger than several pixels

D: Not widely available in literature but theoretically should be a potential use

E: Not feasible

Source: [1]. Joyce, Karen E., et al. "A review of the status of satellite remote sensing and image processing techniques for mapping natural hazards and disasters." *Progress in Physical Geography* 33.2 (2009): 183-207.